nature communications

Article

https://doi.org/10.1038/s41467-025-57384-7

APC/C-mediated ubiquitylation of extranucleosomal histone complexes lacking canonical degrons

Received: 14 June 2024

Accepted: 20 February 2025

Published online: 15 March 2025

Check for updates

Aleksandra Skrajna[1,2,9,10], Tatyana Bodrug[2,3,10], Raquel C. Martinez-Chacin[2,4], Caleb B. Fisher[3], Kaeli A. Welsh[4], Holly C. Simmons[1], Eyla C. Arteaga[1], Jake M. Simmons[1,3], Mohamed A. Nasr[5], Kyle M. LaPak[6], Anh Nguyen[6], Mai T. Huynh[1], Isabel Fargo[1], Joshua G. Welfare[1], Yani Zhao[1], David S. Lawrence[1,4,7], Dennis Goldfarb[5,8], Nicholas G. Brown[2,4] & Robert K. McGinty[1,2,3]

Non-degradative histone ubiquitylation plays a myriad of well-defined roles in the regulation of gene expression and choreographing DNA damage repair pathways. In contrast, the contributions of degradative histone ubiquitylation on genomic processes has remained elusive. Recently, the APC/C has been shown to ubiquitylate histones to regulate gene expression in pluripotent cells, but the molecular mechanism is unclear. Here we show that despite directly binding to the nucleosome through subunit APC3, the APC/C is unable to ubiquitylate nucleosomal histones. In contrast, extranucleosomal H2A/H2B and H3/H4 complexes are broadly ubiquitylated by the APC/C in an unexpected manner. Using a combination of cryo-electron microscopy (cryo-EM) and biophysical and enzymatic assays, we demonstrate that APC8 and histone tails direct APC/C-mediated polyubiquitylation of core histones in the absence of traditional APC/C substrate degron sequences. Taken together, our work implicates APC/C-nucleosome tethering in the degradation of diverse chromatin-associated proteins and extranucleosomal histones for the regulation of transcription and the cell cycle and for preventing toxicity due to excess histone levels.

The eukaryotic genome is packaged in a polymeric complex called chromatin. The repeating unit of chromatin, the nucleosome, consists of an octameric core assembled from a central H3/H4 tetramer and two H2A/H2B dimers, wrapped by ~145 bp of DNA[1,2]. Histone proteins display diverse post-translational modifications that regulate genomic processes[3]. One such modification, ubiquitylation, has been documented on all four core histone proteins[4,5]. Ubiquitin is attached through its C terminus to substrate lysine side chains through an

[1]Division of Chemical Biology and Medicinal Chemistry and Center for Integrated Chemical Biology and Drug Discovery, UNC Eshelman School of Pharmacy, University of North Carolina, Chapel Hill, NC, USA. [2]Lineberger Comprehensive Cancer Center, University of North Carolina, Chapel Hill, NC, USA. [3]Department of Biochemistry and Biophysics, UNC School of Medicine, University of North Carolina, Chapel Hill, NC, USA. [4]Department of Pharmacology, UNC School of Medicine, University of North Carolina, Chapel Hill, NC, USA. [5]Curriculum in Genetics and Molecular Biology, University of North Carolina, Chapel Hill, NC, USA. [6]Department of Cell Biology and Physiology, Washington University School of Medicine, St. Louis, MO, USA. [7]Department of Chemistry, University of North Carolina, Chapel Hill, NC, USA. [8]Institute for Informatics, Washington University School of Medicine, St. Louis, MO, USA. [9]Present address: Department of Chemistry and Biochemistry, University of California, Santa Cruz, CA, USA. [10]These authors contributed equally: Aleksandra Skrajna, Tatyana Bodrug. e-mail: nbrown1@med.unc.edu; rmcginty@email.unc.edu

enzymatic cascade of E1 ubiquitin-activating enzymes, E2-ubiquitin conjugating enzymes, and E3 ubiquitin ligases[6]. Ubiquitylation can result in substrate degradation or signaling events depending on the ubiquitin chain length and linkage pattern and the number of lysines ubiquitylated[6–9].

Despite a growing appreciation of diverse roles of non-degradative histone ubiquitylation in gene expression and genome integrity[4,5], the roles of degradative histone ubiquitylation and any contributions to nuclear homeostasis or genome function are poorly understood. This is an important knowledge gap given the toxicity associated with excessive levels of histone proteins[10,11]. In *S. cerevisiae*, homeostasis of H3 outside of chromatin is controlled by phosphorylation and ubiquitin-dependent degradation[12]. DNA damage is also linked with core and linker histone ubiquitylation by several E3 ligases and broad loss of histone occupancy[13,14]. In metazoans, ubiquitin-independent proteasomal histone degradation has been described in DNA repair and spermatogenesis through recognition of acetylated histones[15]. Early evidence of ubiquitin-dependent histone degradation in metazoans is emerging[16]. One clear example is RNF8 mediated H3K4 polyubiquitylation regulating gene expression in response to EGFR stimulation[17]. In other cases, histone levels have been shown to be regulated by the ubiquitin-proteasome system and some important steps have been identified but molecular details including the E3 ligases involved are not known[18–21]. A lack of clearly defined mechanisms for histone destruction is in stark contrast to well documented and precise control of histone synthesis at transcription, mRNA processing, and translation stages[22].

Recently, Anaphase Promoting Complex/Cyclosome (APC/C)-mediated polyubiquitylation of histones was reported to function together with chromatin regulator WDR5 and the basal transcription machinery protein TBP (TATA-box binding protein) to maintain post-mitotic transcriptional profiles necessary for pluripotency in stem cells[23]. Concurrently, we identified the APC/C as a direct nucleosome interactor[24]. APC/C nucleosome binding is dependent on the nucleosome acidic patch, a common hub for hundreds of nucleosome interactions (Fig. 1a)[24,25]. The APC/C is a 1.2 megadalton RING E3 ubiquitin ligase that controls the cell cycle through precisely timed polyubiquitylation and subsequent destruction of cell cycle regulatory proteins[26,27]. Two ubiquitin-conjugating enzymes (E2s), UBE2C and UBE2S, are responsible for priming ubiquitylation and ubiquitin chain elongation, respectively[28–33]. Interestingly, nearly all other E3 ligases that ubiquitylate nucleosomal histones bind the acidic patch and their histone site-specificity is determined by how the E3 orients on the acidic patch to position the E2 relative to the nucleosome structure[34–37]. Despite growing evidence linking APC/C function to chromatin regulation, the molecular mechanisms governing its nucleosome targeting remain unclear[26,38–40].

Here we show that the APC/C binds the acidic patch using its APC3 subunit but is unable to ubiquitylate nucleosomal histones. Rather, the APC/C ubiquitylates extranucleosomal H3/H4 and H2A/H2B

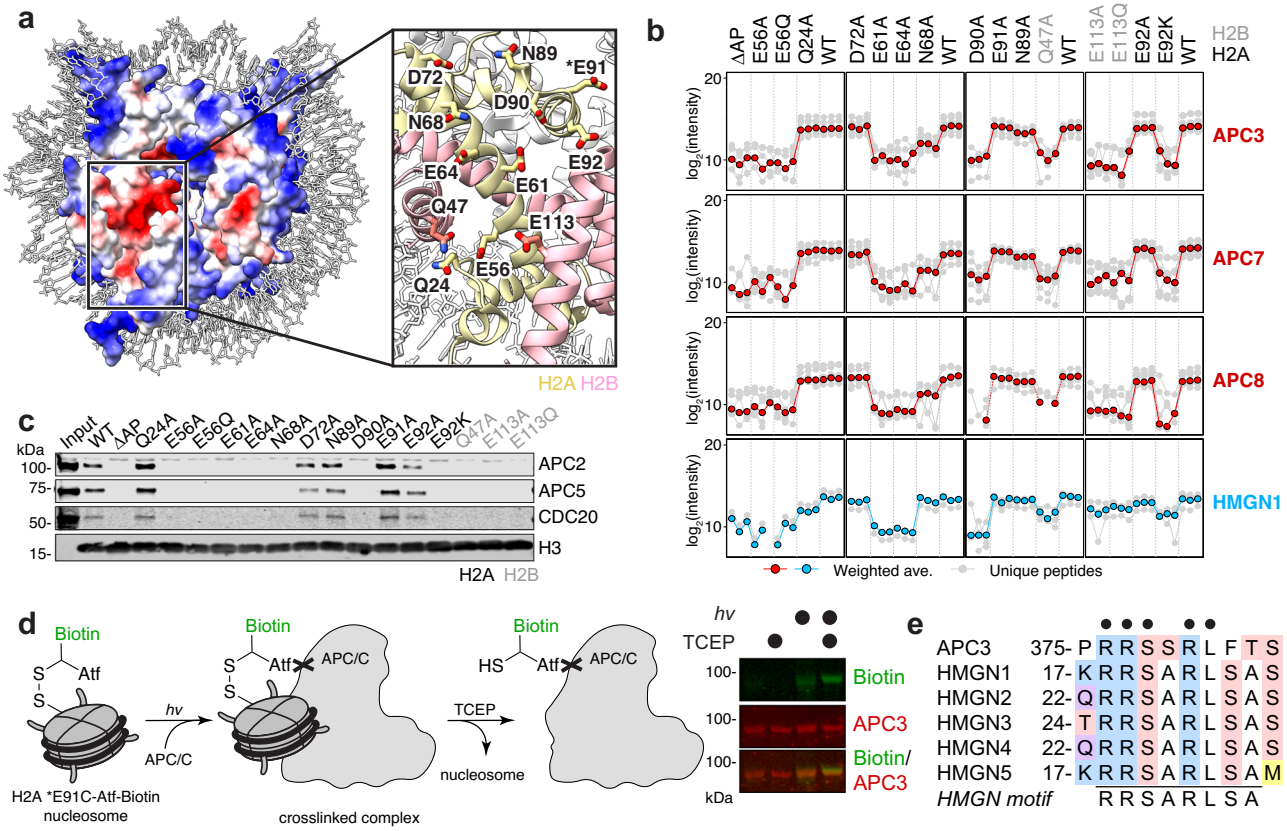

Fig. 1 | APC3 binds nucleosome acidic patch through HMGN-like nucleosome binding motif. a Electrostatic surface of nucleosome (PDB 3AFA), left, and zoomed view of acidic patch showing residues mutated in acidic patch interaction screen, right. **b** Profile plots of APC/C subunits and HMGN1 for triplicate wild-type and mutant nucleosome affinity proteomics experiments (data from[41]). Individual quantitated peptides shown in grey and weighted averages in red or blue. ΔAP: H2A E61A, E64S, N68A, D72S, N89A, D90A, E91S. Additional profile plots shown in Supplementary Fig. 1. **c** Pulldowns from HEK293T nuclear lysates using reconstituted, wild-type or mutant biotinylated nucleosomes followed by western blot for APC2, APC5 or APC/C coactivator, CDC20. Pulldown-westerns performed one time. **d** Schematic of nucleosome label transfer crosslinking experiment with H2A E91C linked to Mts-Atf-Biotin reagent, left. Photocrosslinking followed by TCEP addition, allows transfer of biotin to crosslinked protein. Simultaneous blot for biotin and APC3 consistent with photocrosslinking to APC3. Photocrosslinking performed two times with equivalent results. **e** Sequence alignment of proposed APC3 nucleosome-binding loop and HMGN proteins showing partial conservation of HMGN nucleosome binding motif. Source data are provided as a Source Data file.

complexes through unexpected substrate recognition mechanisms that circumvent traditional APC/C degrons. Our studies have broad implications for how chromatin can recruit E3s such as the APC/C to preferentially template ubiquitylation of chromatin bound targets, especially in the absence of E3-specific degrons, and how extra-nucleosomal histone levels can be tuned to regulate transcription and to mitigate histone toxicity.

Results

APC/C subunit APC3 binds nucleosome acidic patch

We recently used nucleosome affinity proteomics to explore nucleosome acidic patch interactions proteome-wide at amino acid resolution[41]. As part of this study, we quantitated nucleosome binding by eight APC/C subunits (APC1-APC8) to a library of nucleosomes with a single point mutation within the acidic patch or a severe seven amino acid mutation of the acidic patch (ΔAP: H2A E61A, E64S, N68A, D72S, N89A, D90A, E91S). All eight APC/C subunits independently clustered in our dataset due to dramatic loss of binding to nucleosomes with mutations of H2A E56, E61, E64, N68, D90, or E92 or H2B Q47 or E113, representing the largest acidic patch footprint in our dataset (Fig. 1b and Supplementary Fig. 1a). Moreover, principal component analysis showed that APC subunits were among the most influential proteins in driving patterns of acidic patch recognition[41]. To independently confirm our results with an orthogonal approach, we performed pull-downs from HEK293T nuclear lysates with our biotinylated nucleosome library followed by western blots for APC/C subunits APC2 and APC5 or APC/C coactivator CDC20 (Fig. 1c). Consistent with our proteomics results, wild-type nucleosomes pulled down APC/C subunits and CDC20, but nucleosome binding was diminished or undetectable for nearly all mutations, with the few exceptions residing in the periphery of the acidic patch.

Having established the nucleosome requirements for APC/C binding, we next sought to identify the region of the APC/C that interacts with the nucleosome acidic patch. For this purpose, we set up a photocrosslinking system with the Mts-Atf-Biotin label transfer reagent (Fig. 1d). The paucity of cysteines within core histone sequences allowed site-specific attachment of the label transfer reagent through a disulfide bond to an engineered histone cysteine mutant. [The lone cysteine, H3.2 C110, could be mutated to an alanine rendering the nucleosome cysteine-less]. We selected an H2A E91C mutant for attachment of the label transfer reagent due to its proximity to the acidic patch and our observation that E91A mutant nucleosomes retained wild-type interaction with the APC/C (Fig. 1b–d). Following photocrosslinking, the biotin was transferred to crosslinked proteins by reduction of the disulfide linkage with the nucleosome. The Mts-Aft-Biotin reagent restricts crosslinking to an 11 Å radius of E91 allowing precise identification of APC/C subunits near the acidic patch upon APC/C-nucleosome complex formation. We observed light-dependent transfer of Atf-Biotin from the nucleosome to the APC/C through two APC/C subunits based on streptavidin blotting (Fig. 1d and Supplementary Fig. 1b). Simultaneous western blotting confirmed APC3 as one major crosslinked component (Fig. 1d). While our efforts to solve a high resolution cryo-EM structure have been unsuccessful to date, our preliminary 2D classifications of APC/C-nucleosome complexes show additional density originating from the arc lamp region of the APC/C. This density is near the location of the APC3 loops (there are two copies of APC3 in the APC/C), suggestive of nucleosome tethering in this location (Supplementary Fig. 1c). We found that HMGN1, which shares five residues of the HMGN RRSARLSA nucleosome binding motif with the APC3 loop (Fig. 1e), showed similar acidic patch requirements for nucleosome binding (Fig. 1b and Supplementary Fig. 1a) and clustered with APC/C proteins in our nucleosome affinity proteomic study[41–43]. To test if this APC3 loop sequence contributes to nucleosome binding, we assembled a mutant APC/C with the APC3 R376/378/380E triple charge swap mutation (3RE) and performed nucleosome pulldowns. Immobilized APC/C with the APC3 3RE mutation exhibited impaired nucleosome binding (Supplementary Fig. 1d). It is not surprising given the length of the APC3 loop (residues 176-446) and the position of the proposed nucleosome binding motif within the loop (residues 376-381), that conformational heterogeneity would preclude single particle cryo-EM analysis of the APC/C-nucleosome complex.

Reconstituted nucleosomes are not APC/C substrates in recombinant system

We next wanted to explore the role of acidic patch binding on APC/C-mediated nucleosome ubiquitylation. To precisely track histone ubiquitylation, we prepared four nucleosomes, each with one of the core histones labeled with a small molecule fluorophore, Oregon Green 488 (labeled histone annotated with*). To our surprise, we did not observe histone ubiquitylation by an activated polyglutamic acid variant of the APC/C when using CDC20 or CDH1 as a coactivator and E2 UBE2C, despite efficient polyubiquitylation of a control substrate Cyclin B (residues 1-95) (Cyclin B^{N}) (Fig. 2a and Supplementary Fig. 2a). This result is in contrast to a previous report of H2B ubiquitylation of purified, endogenous nucleosomes by APC/C co-immunoprecipitated with WDR5[23]. WDR5 has been proposed to function as a substrate coadaptor for nucleosome ubiquitylation[23]. Importantly, we also observed no nucleosome ubiquitylation upon addition of recombinant WDR5 (Supplementary Fig. 2b). This indicates that unidentified factors co-purifying with endogenous nucleosomes or the APC/C-WDR5 and/or post-translational modifications that are not present in our highly defined, reconstituted system are likely required for nucleosome ubiquitylation.

APC/C ubiquitylates extranucleosomal histones in absence of canonical degrons

Despite not observing nucleosomal histone ubiquitylation, the APC/C robustly ubiquitylated all four core histones in extranucleosomal H3/H4 tetramers and H2A/H2B dimers when using CDC20 or CDH1 as a coactivator (Fig. 2a and Supplementary Fig. 2a). H3/H4 tetramers and H2A/H2B dimers, which are intermediates of nucleosome assembly, are commonly associated with histone chaperone proteins prior to incorporation into chromatin during DNA replication or upon mobilization from chromatin during transcription and other DNA-templated processes[44]. To probe whether histone chaperone binding prevents histone complex ubiquitylation, we prepared the H2A/H2B*/Nap1 histone chaperone complex. We observed only a modest decrease in H2B ubiquitylation in the H2A/H2B*/Nap1 complex compared to the unbound H2A/H2B* complex (Fig. 2b). Thus, chaperone binding does not, as a rule, protect histone complexes from APC/C-mediated ubiquitylation. Moreover, although nucleosome binding by the APC/C is lost upon mutation of the acidic patch on the H2A/H2B surface (Fig. 1c) or addition of the acidic patch binding peptide LANA[24], the ΔAP H2A/H2B* complex does also serve as substrate for the APC/C albeit at mildly lower activity (Supplementary Fig. 2c). Overall, we conclude that the primary molecular mechanisms of extranucleosomal histone complex recognition by the APC/C are unique from those governing nucleosome binding to the acidic patch.

APC/C substrate selectivity is often dictated by coactivator-dependent interactions with substrate embedded degron motifs, such as KEN- and D-boxes[45]. To identify potential degron mechanisms required for H2A/H2B and H3/H4 ubiquitylation, we repeated APC/C assays in the presence of unlabeled D-box and or KEN-box containing peptides from the APC/C substrate HSL1[46] that disrupt ubiquitylation of D-box containing Cyclin B and D-box and KEN-box containing Securin substrates (Supplementary Fig. 2d). No HSL1-mediated inhibition was observed when using H2A/H2B dimers as a substrate; in fact, a paradoxical increase in ubiquitylation occurred upon addition of the HSL1 D-box peptide (Fig. 2c). For H3/H4 tetramers, the HSL1 peptides

https://doi.org/10.1038/s41467-025-57384-7

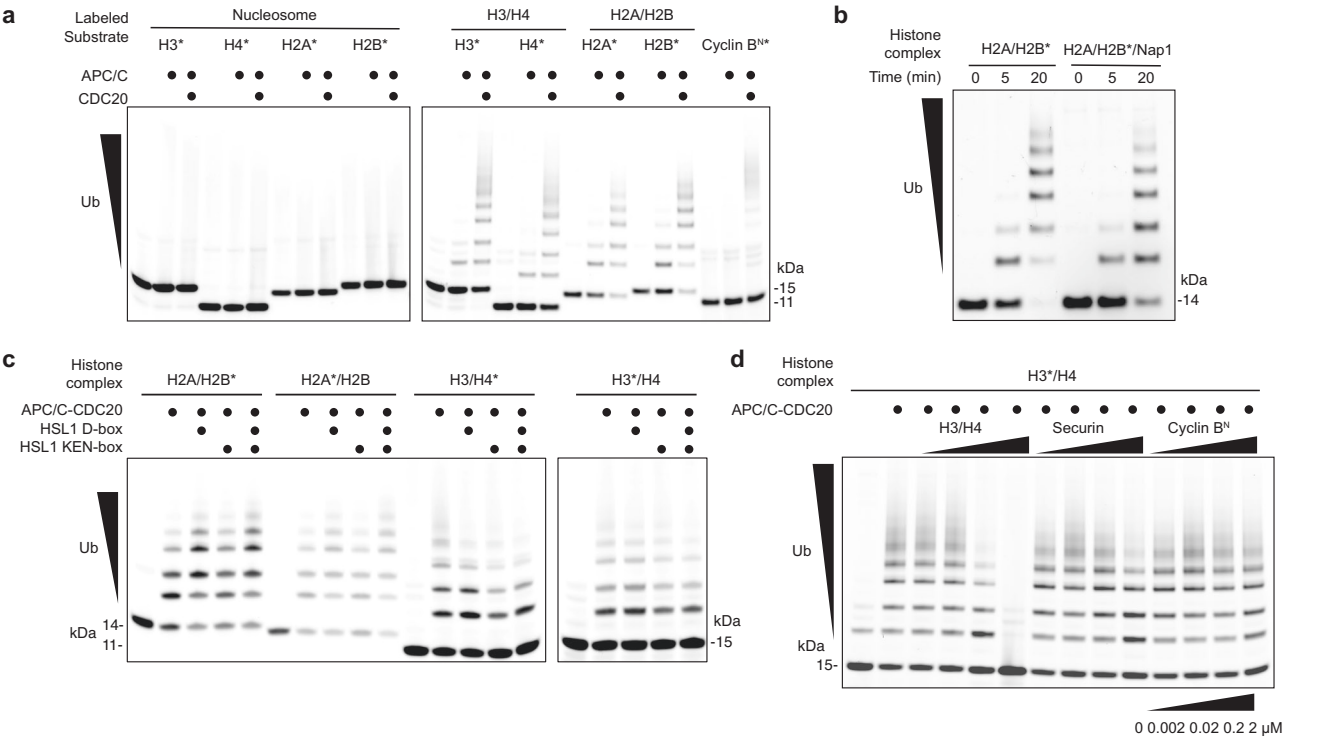

Fig. 2 | APC/C ubiquitylates extranucleosomal histones in absence of canonical degron. a APC/C-CDC20-mediated ubiquitylation assays using indicated nucleosomes, H3/H4 tetramers, or H2A/H2B dimers assembled with one fluorescently labeled histone indicated with asterisk. Cyclin B^{N*} included as control APC/C substrate. Reactions were visualized by fluorescent scanning of SDS-PAGE gels. Representative images of $n = 3$ independent experiments. **b** Time course of H2B ubiquitylation by APC/C-CDC20 using H2A/H2B* dimer alone or bound to Nap1 histone chaperone as a substrate. Representative image of $n = 4$ independent experiments. **c** APC/C-dependent ubiquitylation assays with indicated substrates and HSL1 D-box and/or HSL1 KEN-box containing peptide competitors. Representative images of $n = 2$ independent experiments. **d** APC/C-mediated ubiquitylation assays with H3*/H4 tetramer substrates titrated with unlabeled H3/H4, Securin, or Cyclin B^N competitor substrates. Representative image of $n = 3$ independent experiments. Source data are provided as a Source Data file.

only resulted in minor decreases in histone ubiquitylation that are inconsistent with competition for degron recognition. Moreover, titration of unlabeled APC/C substrates, Securin and Cyclin B^N, that contain canonical degrons, failed to inhibit H3 ubiquitylation in H3*/H4 tetramers (Fig. 2d). In contrast, an identical concentration of unlabeled H3/H4 tetramers prevented H3*/H4 ubiquitylation. We observed similar inhibition of H2A/H2B* dimers by unlabeled H2A/H2B or ΔAP H2A/H2B dimers but not by Securin (Supplementary Fig. 2e). Unlike H3/H4, H2A/H2B* ubiquitylation was modestly inhibited by titration of Cyclin B^N. Recently, Cyclin B has been demonstrated to interact with the nucleosome acidic patch[47]. As such, we suspect that Cyclin B may weakly inhibit H2A/H2B ubiquitylation through direct histone interaction and thus a degron independent mechanism. Altogether, these results demonstrate that the APC/C targets all four core histones in extranucleosomal complexes through mechanisms distinct from canonical degron motifs.

APC/C ubiquitylates lysines in both the histone-fold and tail regions

Having established extranucleosomal H3/H4 and H2A/H2B complexes as robust APC/C substrates, we wanted to identify the sites of histone ubiquitylation. Core histone proteins adopt characteristic α1-L1-α2-L2-α3 histone folds[1,2]. Extensions protrude from the histone fold and include folded regions and disordered tails, which are the sites of many histone post-translational modifications[3]. All four core histones have disordered N-terminal tails and H2A has an additional disordered C-terminal tail with all tails rich in lysines. To determine if the APC/C ubiquitylates folded histone regions or unstructured tails, we prepared four histone complexes, each containing one fluorescently labeled, tailless histone: H3(44-135)*/H4 ($H3^{\Delta N}$*/H4), H3/H4(31-102)* (H3/$H4^{\Delta N}$*), H2A(27-97)*/H2B ($H2A^{\Delta NC}$*/H2B), and H2A/H2B(36-125)* (H2A/$H2B^{\Delta N}$*) (Fig. 3a). Notably, the tailless histone truncations were designed based on expected tails in H3/H4 tetramers and H2A/H2B dimers, which in some cases are longer than the corresponding tails in the context of the nucleosome. We observed decreased ubiquitylation for each tailless histone complex compared to full-length controls (Fig. 3a). This observation was most dramatic for $H2A^{\Delta NC}$/H2B and H2A/$H2B^{\Delta N}$ dimers which were restricted to mono- and diubiquitylation. Yet, in all cases, tailless histone ubiquitylation was observed. This shows that while many sites of histone ubiquitylation reside in disordered tail regions, folded histone regions are also targeted by the APC/C.

To identify specific sites of ubiquitylation, we scaled up APC/C ubiquitylation of H3/H4 or H2A/H2B substrates in reactions that included 10% of fluorescently labeled H3/H4* or H2A/H2B* for monitoring reaction progress, and contained either ubiquitin (Ub) or methylated ubiquitin (meUb), to allow (Ub) or impede ubiquitin chain formation (meUb) (Supplementary Fig. 3). In these reactions, multi-monoubiquitylation of H4 (up to 4) and H2B (above 10) is observed in the meUb samples. We enriched histone complexes from reaction mixtures using a cation exchange resin prior to trypsin digestion and LC-MS analysis of histone peptides containing an isopeptide linked di-glycine remnant of an attached ubiquitin. In agreement with our tailless histone assays, we identified many ubiquitylation sites in H3 and H4 within both histone tails and folded domains (Fig. 3b and Supplementary Data 1). Fewer sites were identified in H2A and H2B, and with one exception, were restricted to disordered tail regions. Importantly, we observed H4 peptides containing up to three ubiquitin di-glycine remnants indicating localized multi-monoubiquitylation that is consistent with observed poly-meUb (Supplementary Fig. 3).

https://doi.org/10.1038/s41467-025-57384-7

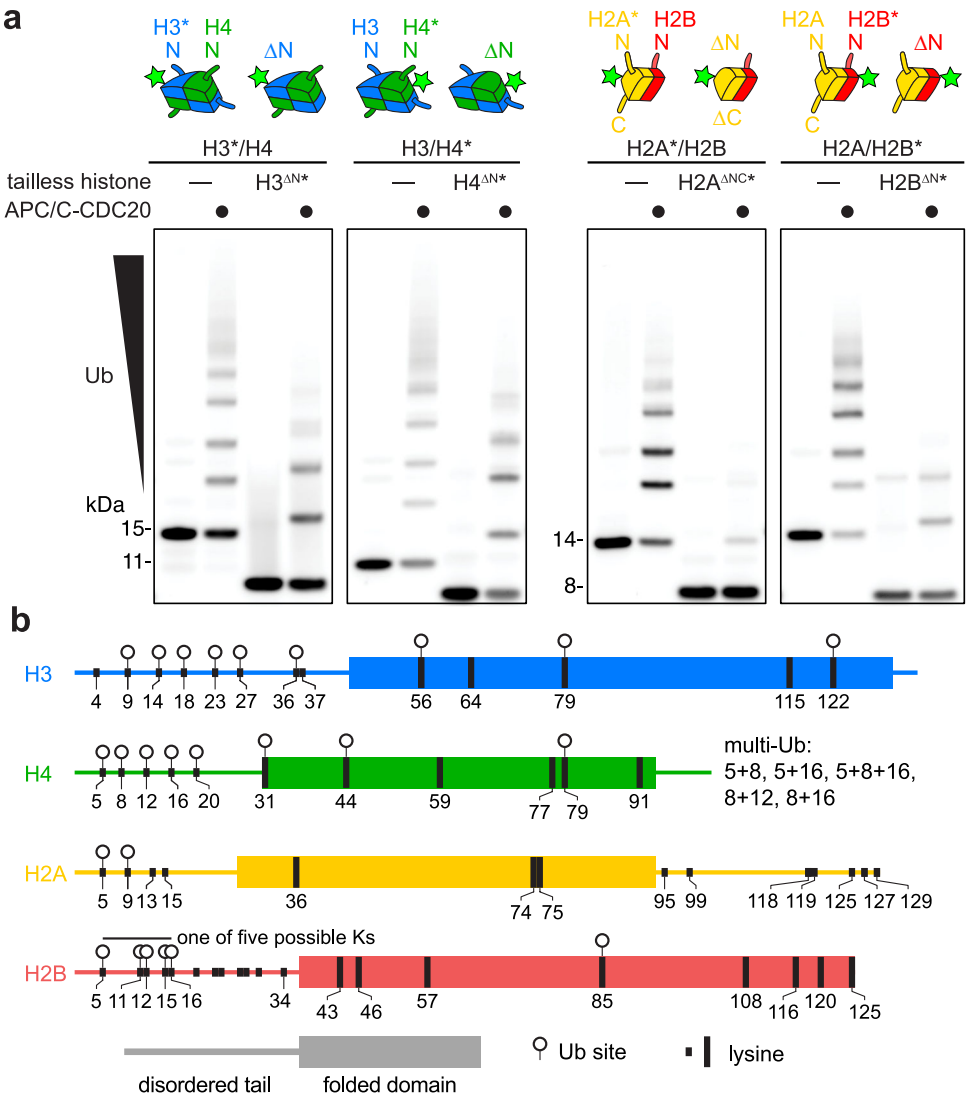

Fig. 3 | APC/C ubiquitylates histone tails and folded domains. a APC/C-mediated ubiquitylation assays using indicated tailless histone substrates visualized by fluorescent scanning of SDS-PAGE gels. Representative images of $n = 2$ experiments. **b** Schematic of mass spectrometry identified ubiquitylation sites (open circles) mapped onto histone structures with tails and folded histone regions and the position of all lysines annotated. Source data are provided as a Source Data file.

APC/C-CDC20-histone complex structures mimicking histone ubiquitylation

Given that histone complexes serve as substrates for the APC/C in the absence of canonical degron sequences, we wanted to visualize the APC/C in the act of histone H3/H4 and H2A/H2B ubiquitylation to better understand molecular mechanisms of histone recognition. To facilitate stable APC/C-CDC20-UBE2C-H2A/H2B and -H3/H4 complex formation for single particle cryo-electron microscopy (cryo-EM), we prepared crosslinked UBE2C-X-H3/H4 and UBE2C-X-H2A/H2B E2-substrate complexes. We selected one ubiquitylation site in each histone complex, H3 K27 and H2B K11, for mutation to cysteine, allowing site-specific crosslinking of each histone complex to the active site C114 in UBE2C with bismaleimidoethane (BMOE) (Fig. 4a, b)[48–50]. When bound to APC/C-CDC20, these crosslinked complexes mimic substrate recognition during ubiquitylation. Importantly, titration of the BMOE-crosslinked UBE2C-X-H3/H4 and UBE2C-X-H2A/H2B complexes inhibited ubiquitylation of Cyclin B to a greater degree than the histone complexes alone, while no inhibition was observed with UBE2C(C114S) -Ub conjugates (Supplementary Fig. 4). This indicates additional points of contact between the histones and APC/C-CDC20.

We reconstituted and purified APC/C-CDC20-UBE2C-X-H3/H4 and -X-H2A/H2B complexes using size exclusion chromatography (Fig. 4a, b). The complexes were glutaraldehyde crosslinked and subjected to single particle cryo-EM analysis allowing 3D reconstructions at ~4 Å resolution (Supplementary Figs. 5–6 and Supplementary Table 1). We could confidently model APC/C-CDC20-UBE2C into our cryo-EM maps. Additional density matching the size and shape of a histone heterodimer exists adjacent to UBE2C and CDC20 in the APC/C central catalytic cavity (Fig. 4a, b). Despite extensive focused refinement, this extra density lacked well defined features, likely due to conformational heterogeneity, which limited high confidence modeling of the exact orientation of the histone complexes (Supplementary Figs. 5–6). However, representative heterodimeric models of H3/H4 and H2A/H2B fit well within the additional density (Fig. 4a, b and Supplementary Fig. 7). Interestingly, both H3/H4 and H2A/H2B densities span the APC/C catalytic cavity and are continuous with APC8. We suspect that the histone complexes are flexibly tethered at one end through UBE2C crosslinking and at the other end, through non-covalent interactions with APC8. This would allow rotation of the histone complexes relative to the APC/C, while restricting the complexes to the APC/C catalytic cavity. In the case of the APC/C-CDC20-UBE2C-H3/H4 complex, rotation of the tethered H3/H4 heterodimer would result in further blurring of the other half of the tetrameric histone complex in EM reconstructions. Notably, real space refinement

https://doi.org/10.1038/s41467-025-57384-7

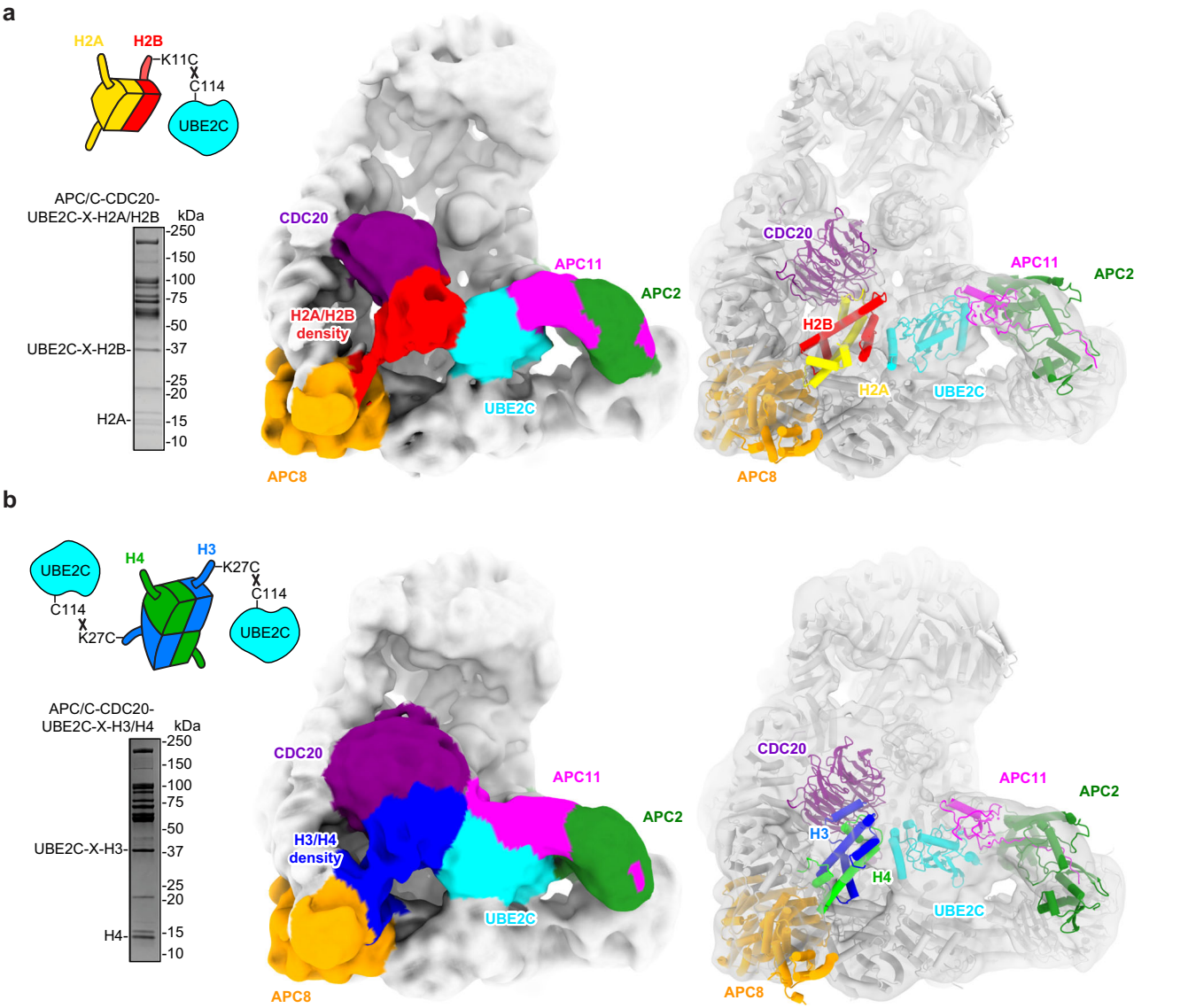

Fig. 4 | Cryo-EM models of APC/C-CDC20-UBE2C-X-H2A/H2B and -X-H3/H4 complexes. a Schematic of UBE2C-X-H2A/H2B crosslinked E2-X-substrate complex, top left. UBE2C C114 crosslinked to H2B K11C mutant using BMOE. Representative image of Coomassie-stained gel of reconstituted APC/C-CDC20-UBE2C-X-H2A/H2B complex, bottom left. Cryo-EM map low pass filtered at 10 Å resolution to visualize density in APC/C central cavity, middle, and proposed model overlaid with map, right, of APC/C-CDC20-UBE2C-X-H2A/H2B complex. **b** Schematic of UBE2C-X-H3/H4 crosslinked E2-X-substrate complex, top left. UBE2C C114 crosslinked to H3 K27C mutant using BMOE. Gel of reconstituted APC/C-CDC20-UBE2C-X-H3/H4 complex, bottom left. Cryo-EM map low pass filtered at 10 Å resolution to visualize density in APC/C central cavity, middle, and proposed model overlaid with map, right, of APC/C-CDC20-UBE2C-X-H3/H4 complex. One H3/H4 heterodimer is modeled. Gels is (**a**, **b**) completed once. Source data are provided as a Source Data file.

repositioned UBE2C and CDC20 from locations in initial docked models generated from PDB ID 8TAU and 6Q6H. The final models more closely align with PDB ID 5KHR and 5L9U which employed similar UBE2C crosslinking strategies to visualize APC/C substrate recognition (Supplementary Fig. 8)[49–53].

Coactivator-dependent and -independent APC/C binding and histone ubiquitylation

One clear difference between the APC/C-CDC20-UBE2C-X-H3/H4 and -X-H2A/H2B complexes is the stoichiometry of the histone complexes. Since H3/H4 forms a tetramer, each UBE2C-X-H3/H4 complex contains two H3/H4 heterodimers, each crosslinked to UBE2C. This is in contrast to UBE2C-X-H2A/H2B which includes only one histone heterodimer and therefore one UBE2C per complex. This distinction is evident in cryo-EM 2D classifications showing APC/C dimerization in UBE2C-X-H3/H4 samples that were not observed with matched UBE2C-X-H2A/H2B complexes (Fig. 5a and Supplementary Figs. 5–6). APC/C dimerization could result from direct interactions with UBE2C and/or H3/H4. To directly probe the role of H3/H4 interactions in APC/C dimerization, we performed mass photometry with the APC/C in the absence of a coactivator and looked for changes in complex size upon addition of H3/H4 tetramers or H2A/H2B dimers that were not crosslinked to UBE2C. The APC/C alone formed a narrow distribution of sizes matching the monomeric APC/C molecular weight (Fig. 5b and Supplementary 9a). Addition of H3/H4 tetramers resulted in a dose dependent shift in the size distribution to include APC/C dimers (Fig. 5b and Supplementary Fig. 9a). The histone tails are required for APC/C dimerization, which was not observed upon titration of $H3^{\Delta N}$/$H4^{\Delta N}$ tailless tetramers. There was no apparent change in the APC/C size in the presence of H2A/H2B dimers. This observation rules out APC/C dimerization by H2A/H2B but does not report on APC/C-H2A/H2B complex formation due to limitations in detecting a 28 kDa

https://doi.org/10.1038/s41467-025-57384-7

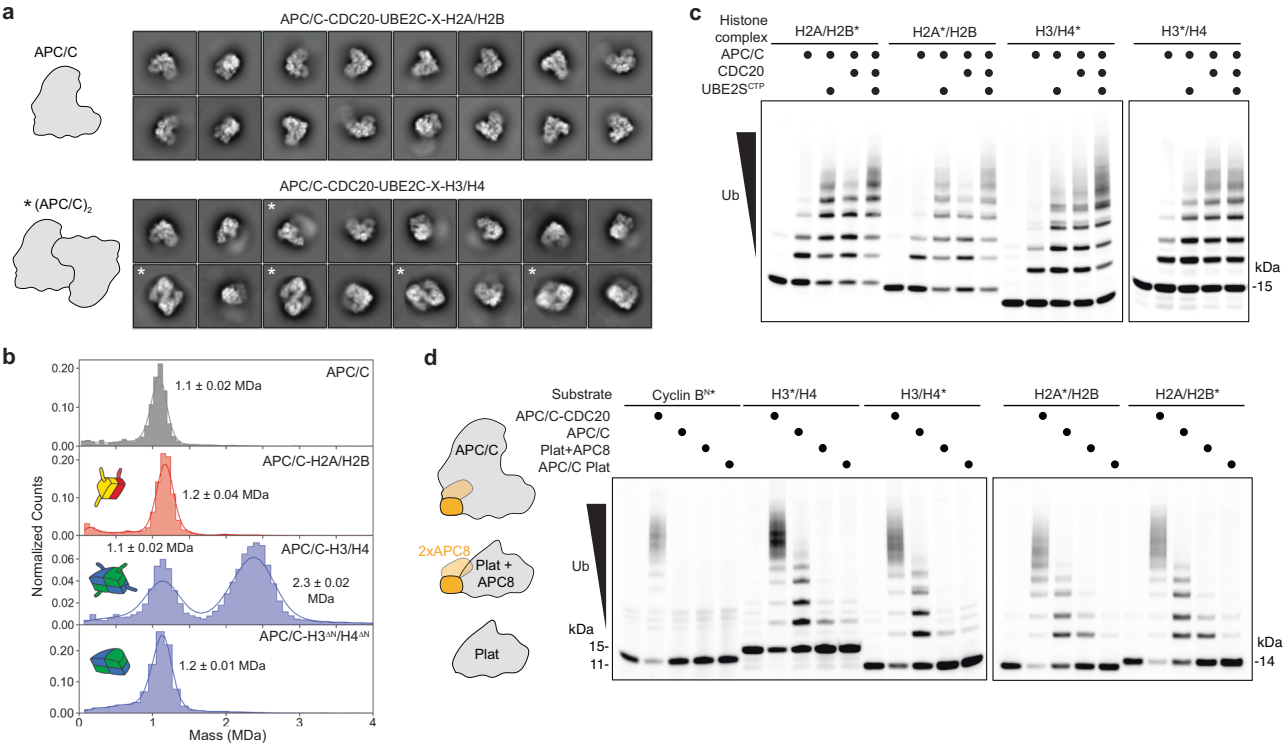

Fig. 5 | APC8 contributes to coactivator-independent histone complex ubiquitylation. a Representative 2D classes of APC/C-CDC20-UBE2C-X-H2A/H2B and -X-H3/H4 showing absence and presence of APC/C dimers, respectively. **b** Representative mass photometry histograms of APC/C alone or in complex with 320 nM H2A/H2B dimers or H3/H4 tetramers with and without N-terminal tails, demonstrating H3/H4-mediated APC/C dimerization. Additional replicates and concentrations are shown in Supplementary Fig. 9a. **c** APC/C-dependent ubiquitylation assays of indicated histone complexes in the presence of coactivator CDC20 and/or the activating UBE2S^{CTP}. Representative images of $n = 3$ experiments. **d** Ubiquitylation assays of indicated histone complexes using APC/C platform (Plat), APC Plat + APC8, APC/C or APC/C-CDC20. Representative images of $n = 3$ experiments. Assays is (**c**, **d**) visualized by fluorescent scanning of SDS-PAGE gels. Source data are provided as a Source Data file.

change in a 1.2 MDa complex by mass photometry. Therefore, we reconstituted APC/C-H2A/H2B* complexes with and without CDC20 and analyzed stable complex formation by size exclusion chromatography. H2A/H2B* coeluted with both APC/C and APC/C-CDC20 complexes with the expected 1:1 APC/C:H2A/H2B stoichiometry (Supplementary Fig. 9b). Overall, we conclude that H3/H4 and H2A/H2B interact directly with the APC/C and a coactivator is not a requisite for APC/C binding.

Our initial enzymatic assays showed low levels of histone complex ubiquitylation in the absence of a coactivator, especially for H2A and H2B and histone ubiquitylation was increased by addition of CDC20 or CDH1 (Fig. 2a and Supplementary Fig. 2a). CDC20 and CDH1 enhance APC/C-mediated ubiquitylation through two mechanisms, direct substrate recruitment and promoting an upward, active conformation of the APC2-APC11 catalytic core[48,51,52]. We recently demonstrated that the UBE2S C-terminal peptide (UBE2S^{CTP}, residues 204-222), also activates the APC/C catalytic core, bypassing the activation capacity of the coactivators[51,54]. The UBE2S^{CTP} boosted ubiquitylation of H2A and H2B to levels higher than observed with CDC20, and modest synergy was observed upon addition of both the UBE2S^{CTP} and CDC20 (Fig. 5c). We obtained similar results with H3 and H4 albeit with slightly reduced UBE2S^{CTP} activation compared to CDC20. These results further support both coactivator-dependent and -independent recognition of histone complex substrates.

APC8 promotes histone ubiquitylation

In order to determine the region(s) of the APC/C required for histone complex recognition, we tested whether subcomplexes of the APC/C retained the ability to ubiquitylate H3/H4 tetramers and H2A/H2B dimers. The APC/C can be loosely divided into two regions: a platform that includes the APC2-APC11 catalytic core and an arc lamp that extends up from the platform to complete the central catalytic cavity[26]. The APC/C platform (APC/C Plat) pairs with UBE2C to weakly ubiquitylate all four histones within H3/H4 tetramers and H2A/H2B dimers (Fig. 5d). As our cryo-EM reconstructions showed H3/H4 and H2A/H2B density in the central catalytic cavity continuous with APC8, we tested whether addition of APC8 to the platform (APC/C Plat + APC8) could promote histone ubiquitylation. APC8 strongly enhanced H2A/H2B ubiquitylation (Fig. 5d). We observed smaller APC8-depedent increases in H3/H4 ubiquitylation that importantly were not observed with control substrate Cyclin B^{N}. We conclude that APC8 is important for histone complex recognition, but the different levels of APC8-dependent ubiquitylation observed may reflect distinct H3/H4 and H2A/H2B binding mechanisms and/or consequences of APC/C dimerization.

H2A tail pairs with APC8 to direct H2B ubiquitylation

In the APC/C-CDC20-UBE2C-X-H2A/H2B complex, H2B K11C is covalently tethered to UBE2C C114. This would prevent the same H2B N-terminal tail from simultaneous interaction with APC8, which at its closest point is 55 Å away (Fig. 6a). Therefore, we hypothesized that an H2A tail could bind APC8 to present H2B for ubiquitylation. To test this hypothesis, we prepared H2A/H2B dimers with one tailless histone and the other histone full-length and fluorescently labeled, allowing us to examine the importance of the tail(s) of one histone on the ubiquitylation of its heterodimeric partner. We observed only a modest decrease in H2A ubiquitylation in H2A*/H2B$^{\Delta N}$ dimers (Fig. 6b). In contrast, H2B ubiquitylation was severely limited in H2A$^{\Delta NC}$/H2B* dimers compared to full-length controls. We next probed the contributions of H2A N- and C-terminal tails individually. The H2A$^{\Delta N}$

https://doi.org/10.1038/s41467-025-57384-7

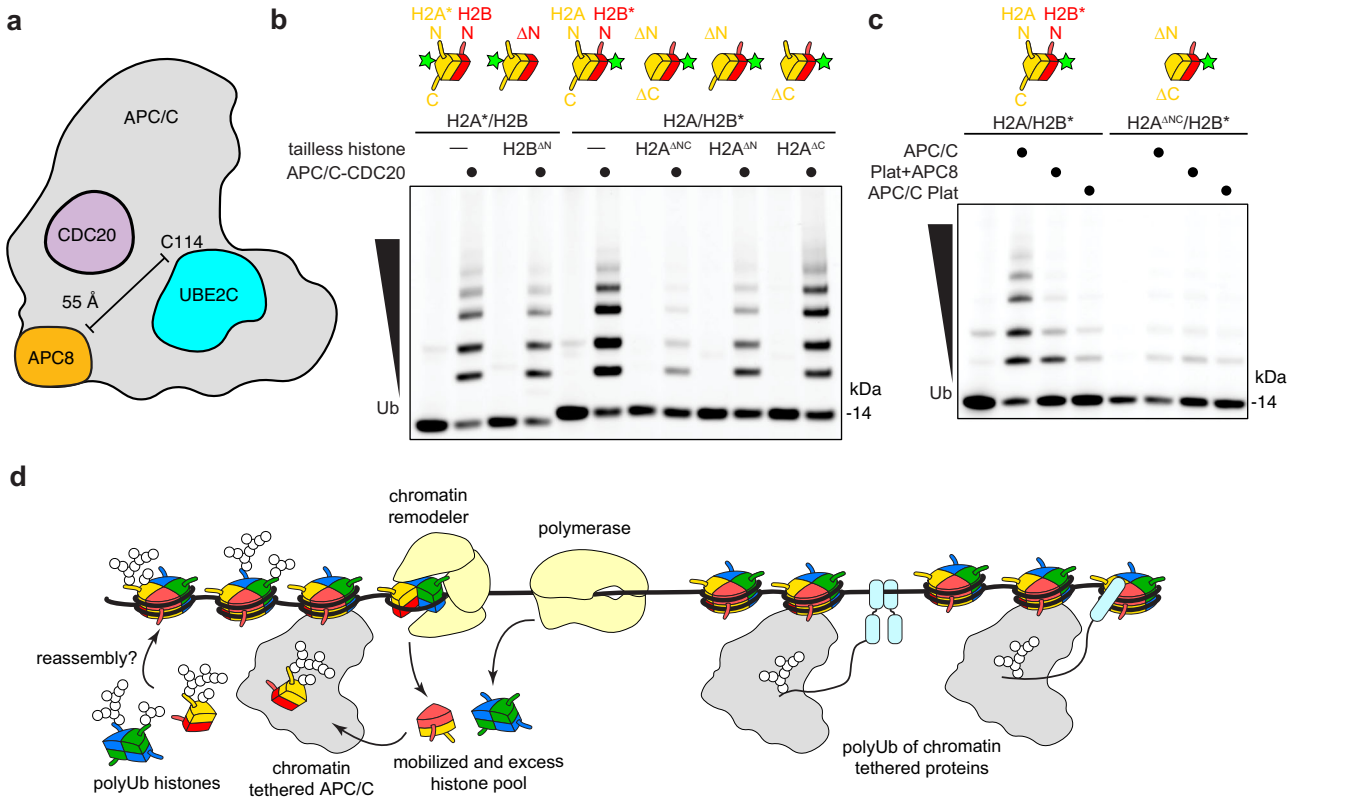

Fig. 6 | H2A disordered tails are required for APC8-dependent H2B ubiquitylation. a Schematic of APC/C architecture highlighting distance between APC8 and UBE2C active site cysteine, C114. **b** APC/C-mediated ubiquitylation assays using H2A/H2B dimers with one histone fluorescently labeled and the other histone tailless visualized by fluorescent scanning of SDS-PAGE gels. Representative image of $n = 3$ experiments. **c** Ubiquitylation assays of H2B in the context of H2A tail truncations using APC/C platform (Plat), APC Plat + APC8, APC/C or APC/C-CDC20. Representative image of $n = 3$ experiments. **d** Model of chromatin-tethered APC/C polyubiquitylating histones mobilized by polymerases or chromatin remodeling complexes, left, or DNA or nucleosome bound proteins, right. Source data are provided as a Source Data file.

truncation led to decreased H2B ubiquitylation but was less severe than truncation of both tails, showing that the H2A N-terminal tail is a primary determinant of H2B ubiquitylation with additive contribution of the C-terminal tail (Fig. 6b). Moreover, the H2A(1–26) N-terminal tail peptide inhibits H2A*/H2B but not Cyclin B^N ubiquitylation in a dose-dependent manner (Supplementary Fig. 10a). A similar pattern of inhibition of H3/H4* ubiquitylation was observed using the H3(1-43) N-terminal tail peptide (Supplementary Fig. 10b). Finally, we probed the ubiquitylation of H2A/H2B* and $H2A^{\Delta NC}$/H2B* dimers by APC/C Plat with and without APC8. We observed similar low levels of H2B ubiquitylation by the APC/C Plat when in complex with full-length or N-tailless H2A. However, APC8-mediated H2B ubiquitylation was only observed in the presence of the full-length H2A (Fig. 6c). Altogether, our data suggests that the H2A N-terminal tail pairs with APC8 for non-canonical substrate recognition of H2A/H2B complexes.

Discussion

Here, we have shown that the APC/C binds to but is unable to ubiquitylate nucleosomes, despite robust ubiquitylation of extra-nucleosomal histone complexes. This would enable multiple roles of the APC/C in regulating chromatin processes spanning gene regulation, cell cycle control, and histone homeostasis: (1) nucleosome-tethering of the APC/C to facilitate polyubiquitylation and degradation of chromatin-associated substrates, without broadly degrading histones that are safeguarded by nucleosome incorporation, (2) locus-specific degradation of mobilized histones to dictate chromatin accessibility for transcription and other genomic processes, and (3) restriction of toxic levels of extranucleosomal histones in coordination with the cell cycle.

We previously identified the APC/C as a direct nucleosome acidic patch binding complex[24]. We have now extended this analysis to map the molecular footprint of the APC/C on the acidic patch at amino acid resolution through nucleosome pulldown mass spectrometry and western blot analysis. Most nucleosome interacting proteins engage the acidic patch using one or more arginines, termed arginine anchors and variant arginines based on their binding locations[25]. The broad acidic patch footprint of the APC/C suggests use of an arginine anchor, which inserts into the H2A E61/D90/E92 cavity, as well as two variant arginines, one requiring H2A E56A and H2B E113, and the other, H2A E64. We observed photocrosslinking between APC3 and a label transfer reagent attached to the nucleosome at H2A E91, demonstrating that APC3 is within 11 Å of the acidic patch. The acidic patch binding requirements for APC/C subunits and HMGN1 were nearly identical in our nucleosome affinity proteomics screen[41]. HMGN1 binds the acidic patch using an invariant RRSARLS nucleosome binding motif[42]. Notably, the arginine-rich sequence in the APC3 loop shares five of seven HMGN motif residues, including all three arginines. Mutation of the three arginines in this HMGN motif of APC3 led to a decrease in nucleosome binding. While our cryo-EM efforts with APC/C-nucleosome complexes have thus far been unsuccessful, we observed additional EM density in the arc lamp region of the APC/C near the origin of the APC3 loops—there are two copies of APC3 per complex—consistent with a flexibly tethered nucleosome. Notably, while our manuscript was in revision, a cryo-EM structure of the same APC3 loop peptide bound to the nucleosome, together with crosslinking mass spectrometry data, was published establishing a molecular mechanism of the arginine-acidic patch interactions[47].

Given previous reports of direct ubiquitylation of purified nucleosomes by immunoprecipitated APC/C[23], we were surprised to find that we could not reproduce this activity using recombinant APC/C and reconstituted, unmodified nucleosomes as a substrate, even in the presence of proposed substrate coadaptor, WDR5. One possible explanation is that one or more histone post-translation modifications (PTMs) present in endogenous, purified nucleosomes or the APC/C are necessary for ubiquitylation. For example, pre-existing histone ubiquitylation, estimated at 10% of H2A K119 and 1% of H2B K120[55,56], could prime further nucleosome ubiquitylation by the APC/C. Alternatively, unidentified accessory factors that copurify with WDR5 and the APC/C may facilitate nucleosome modification. As proposed for WDR5, such accessory factors could act as substrate coadaptors, allowing direct nucleosome ubiquitylation. Similarly, the APC/C is extensively modified by post-translational modifications (PTMs), including phosphorylation and sumoylation during mitosis[57–62]. While our version of the APC/C used in these experiments mimics mitotic phosphorylation, some combination of PTMs could play a role in facilitating nucleosome ubiquitylation. Importantly, either mechanism would enable regulated degradation of histones and limit catastrophic, unregulated histone loss. It is also possible that decreased stability of endogenously purified nucleosomes due to histone PTMs or genomic DNA, as opposed to optimized positioning sequences used in our reconstituted nucleosomes could lead to release of H2A/H2B or H3/H4 complexes that we have shown here to be APC/C substrates. Of note, the flanking residues of the APC3 loops are ~190–230 Å from the active center of the APC/C and on the opposite side of the APC/C assembly. The acidic patch binding sequence within the APC3 loop is 66 amino acids from the nearest loop anchor residue 446 and therefore could position the nucleosome near the active center assuming a 3.5 Å distance spanned per residue. This configuration would require tight wrapping of the APC3 loop around much of the APC/C structure, which we predict would be energetically disfavored in the absence of specific APC3 loop interactions with the APC/C that have not been observed previously. N-terminal histone tails range from 15 to 37 amino acids in a nucleosome context and could help span the distance. However, structural studies have demonstrated that histone tails form dynamic and heterogeneous interactions with nucleosomal DNA[63,64] which may further shield nucleosomal histone tails from ubiquitin modification. Thus, we hypothesize given the location of the APC3 loops and the distance from the APC/C active center that acidic patch binding by APC3 may protect nucleosome-incorporated histones from polyubiquitylation.

Chromatin regulatory proteins are highly represented in a growing list of APC/C substrates. These substrates contribute to diverse genomic processes, including transcription (KAT2B, NCOA3, and UHRF1), chromatin assembly (NASP and CHAF1B), RNA processing (LARP1 and LARP7), and DNA damage repair (MSH2)[38]. A recent study demonstrated that Cyclin B, another APC/C substrate and nucleosome-associated protein, is preferentially degraded when associated with chromatin[47]. We expect that the levels of many other chromatin-bound APC/C substrates are regulated across the cell cycle through co-localization on chromatin.

In contrast to nucleosomal histones, the APC/C-UBE2C polyubiquitylates H2A/H2B and H3/H4 complexes in an extranucleosomal context. Extranucleosomal histone pools include newly synthesized replication-dependent and variant histones as well as histones that are ejected from chromatin during dynamic genomic processes. For example, nucleosome remodeling complexes can evict histones or exchange replication dependent and variant histones[65]. This activity is especially important in non-replicative cells that are dependent on replication-independent histone expression for new histone supply. During transcription, nucleosomes are disassembled to allow access to DNA[66–69]. While nucleosomes are typically reassembled after polymerase passage, it is increasingly clear that subnucleosomal particles lacking one or both H2A/H2B are found frequently in actively transcribed chromatin, indicating the formation of extranucleosomal histone complexes[70,71]. Moreover, during DNA damage repair processes such as double strand break repair, histones are evicted to allow repair machineries to function[72]. Regardless of the source, these extranucleosomal histones are thought to exist in H2A/H2B and H3/H4 subcomplexes bound by histone chaperone proteins that both prevent inappropriate histone-DNA interactions but also regulate and facilitate nucleosome (re)assembly[44,73]. We demonstrated that a physiologic chaperone-bound histone complex, H2A/H2B/Nap1, is an APC/C substrate.

Our experiments with methyl-ubiquitin, which prevents formation of ubiquitin chains, suggest that ubiquitylation occurs on multiple sites within the same protein but that polyubiquitin chains are also formed by the priming E2, UBE2C. We identified in excess of 20 ubiquitylation sites within histones, primarily but not exclusively within disordered N-terminal histone tails. Histone tail lysines are densely and diversely modified, influencing local chromatin structure and recruitment or exclusion of chromatin binding factors[3]. Many of the sites that are ubiquitylated by the APC/C can be methylated (e.g., H3 K9, K27, K36, K79 and H4 K20), or acetylated (e.g., H3 K9, K14, K18, K23, K27, K56 and H4 K5, K8, K12, K16, K20). As di- and trimethylation and acetylation are mutually exclusive with acylation, pre-existing patterns of histone modification would be expected to protect specific lysines from APC/C-mediated ubiquitylation. One consequence is that histones derived from different genomic environments with different combinations of PTMs could direct unique APC/C ubiquitylation states. H3 K14, K18, and K23 are also ubiquitylated by the E3 ligase UHRF1, which has been shown to be an APC/C substrate itself. UHRF1 may prime H3 ubiquitylation for APC/C mediated chain extension and in a feedback mechanism, UHRF1 is itself targeted for degradation by the APC/C.

We found H2A/H2B and H3/H4 ubiquitylation to be independent of traditional degrons. While coactivators CDC20 and CDH1 enhanced histone polyubiquitylation, equivalent activation was achieved with the UBE2S^{CTP} activating peptide. Moreover, histone complexes bind nucleosomes in the absence of coactivators, altogether suggesting a non-canonical substrate recognition mechanism. Based on our structures of APC/C-histone complexes and biochemical assays, we propose that APC8-histone tail interactions are a major component of this substrate recognition mechanism. First, histone complexes fill the APC/C central cavity with EM density extending to APC8. Next, APC8 incorporation into the APC/C platform enhances ubiquitylation compared to the APC/C platform alone, especially for H2A/H2B substrates. Finally, the H2A disordered tails are required for efficient H2B ubiquitylation and APC8 stimulation. We hypothesize based on these results and the architecture of the APC/C that a disordered histone tail of one histone protein binds APC8 allowing presentation of other tail(s) in the histone complex for ubiquitylation. This model accounts for larger consequences of histone tail truncations on H2A/H2B dimers than H3/H4 tetramers, with the latter retaining multiple tails when one of the histone subunits is rendered tailless. Distinct substrate behaviors of H3/H4 and H2A/H2B are likely to be compounded by H3/H4 tetramer-mediated APC/C dimerization.

Several APC/C substrates and inhibitors, including NEK2A, Cyclin A, and the CDC20 subunit of the mitotic checkpoint complex (MCC) bind APC8 through hydrophobic-basic dipeptide sequences[50,53,74–76]. However, unlike histone complexes, NEK2A and Cyclin A also contain canonical degron motifs[52,77]. Histone tails are enriched in basic residues but lack clear hydrophobic-basic dipeptide sequences leaving open the possibility of a unique binding mechanism. Importantly, both NEK2A and Cyclin A are degraded in early mitosis. APC/C-mediated H2B ubiquitylation is also highly abundant in early mitosis in pluripotent cells[23]. If extranucleosomal histones are similarly privileged APC/C substrates, it raises the possibility that extranucleosomal histones, rather than nucleosomal histones, are responsible for this

phenomenon. Moreover, as high levels of free histones are toxic to cells[10,11], APC/C-dependent ubiquitylation following S phase may contribute to the elimination of histone complexes that have not been incorporated into chromatin.

Based on all available data, we propose that the APC/C is tethered to chromatin through nucleosome acidic patch interaction. This localizes the APC/C in proximity of DNA- and nucleosome-bound non-histone substrates, favoring their polyubiquitylation and proteasome-mediated degradation (Fig. 6d). Chromatin-tethered APC/C is also poised to polyubiquitylate histones mobilized through dynamic chromatin processes, including chromatin remodeling and transcription. Such polyubiquitylated histone substrates can be targeted for proteasomal degradation directly or after reassembly into chromatin. Such a model would be consistent with polyubiquitylation of extra-nucleosomal, but not nucleosome incorporated, histones in vitro and APC/C-dependent K11-linked polyubiquitylation of histones in mitotic pluripotent cells, allowing targeted destruction of histones near transcription start sites of pluripotency genes and therefore rapid expression upon mitotic exit. More generally, our work suggests that APC/C-mediated ubiquitylation of extranucleosomal histone complexes may contribute to histone homeostasis through restriction of free histone pools.

Methods

Protein purification

The components necessary for APC/C-dependent ubiquitylation and binding assays (human APC/C, CDH1, CDC20, UBA1, UBE2C and UBE2S, and substrates) were generated as described previously[49,78]. Recombinant wild-type and APC3 R376/378/380E (3RE) mutant APC/C and its Platform (APC/C Plat) subcomplexes (APC/C Plat and APC/C Plat +APC8, Plat = APC1, APC2, APC4, APC5, APC11, APC15), as well as CDH1, CDC20, and UBA1 were expressed using baculovirus-infected insect cells. All other components were bacterially expressed in BL21-Codon Plus (DE3)-RIL cells. The oxyester linked UBE2C(C114S)-Ub was prepared using UBE2C(C114S), UBA1, and ubiquitin as previously described[49].

APC/C harboring glutamate substitutions to mimic mitotic phosphorylation[60] was expressed with an N-terminal Twin Strep tag on APC2 and an N-terminal GST tag on APC16. The APC/C is purified by affinity chromatography with Strep-Tactin Sepharose, followed by GST-affinity chromatography, treatment with HRV-3C protease to remove the affinity tags, and a final size-exchange chromatography (SEC) step. SEC was performed in a buffer of 20 mM HEPES pH 8, 200 mM NaCl and 1 mM DTT. The APC/C subcomplexes followed a similar procedure where Strep-Tactin Sepharose was used to initially enrich for the subcomplex using a Twin Strep tag on the C-terminus of APC4. These complexes were then purified by ion-exchange and size-exclusion chromatography as previously described[49].

Peptide sequences from Hsl1, a tight-binding APC/C substrate from S. cerevisiae, where used to examine the binding requirements of the histones. Hsl1 D-box peptide (sequence: QKPKRAALSDITNSFNK) and KEN-box peptide (GVSTNKENEGPEYPTKI) were synthesized, with the N- and C-terminal charges neutralized through acetylation and amidation, respectively.

The mouse Nap1(C88S, C132S, C255S, C258S) (mNap1x1) gene was ordered as a gblock from IDT and cloned into a pST50Tr vector with a TEV protease cleavable N-terminal Strep-10xHis tag. The tagged mNap1x1 was expressed in BL21(DE3)pLysS cells with addition of 0.2 mM IPTG at 18 °C for 16 h. Cells were lysed by sonication and mNap1x1 was purified by Talon metal affinity resin (Takara). Pooled fractions were digested with TEV protease, and further purified using anion exchange chromatography with a Source Q resin (GE Healthcare), followed by size exclusion chromatography using a Superdex 200 increase 10/300 column (GE Healthcare) equilibrated in 20 mM Tris-Cl pH 7.5, 125 mM NaCl, 10 mM 2-mercaptoethanol.

Histone and nucleosome preparation

Bacterial expression plasmids for wild-type human histones, H2AΔAP (H2A E61A, E64S, N68A, D72S, N89A, D90A, E91S), and individual H2A acidic patch mutants (H2A Q24A, E56A, E56Q, E61A, E64A, N68A, D72A, N89A, D89A, D90A, E91A, E92A, E92K; H2B Q47A, E113A, E113Q) were described previously[24,41]. Cysteine point mutant histones (H2A E91C, H2A A10C, H2B A21C, H2B K11C, H3.2 K27C, H3.2 T32C/C110A, H4Q27C) were cloned into pST50Tr bacterial expression vectors by site-directed mutagenesis. Wild type and mutant human histones were expressed in BL21(DE3)pLysS *E. coli*, extracted from inclusions bodies, and refolded into H2A/H2B dimers and H3/H4 tetramers as described previously[24,79]. For histone complexes that were subsequently fluorescently labeled or used for crosslinking, cation exchange purification was performed in the absence of reducing agent. The following full-length histone complexes were prepared: H2A/H2B, H2AΔAP/H2B, H2A(Q24A)/H2B, H2A(E56A)/H2B, H2A(E56Q)/H2B, H2A(E61A)/H2B, H2A(E64A)/H2B, H2A(N68A)/H2B, H2A(D72A)/H2B, H2A(N89A)/H2B, H2A(D90A)/H2B, H2A(E91A)/H2B, H2A(E92A)/H2B, H2A(E92K)/H2B, H2A/H2B(Q47A), H2A/H2B(E113A), H2A/H2B(E113Q), H2AΔAP/H2B(A21C), H2A(E91C)/H2B, H2A(A10C)/H2B, H2A/H2B(A21C), H2A/H2B(K11C), H3.2/H4, H3.2(T32C, C110A)/H4, H3.2(K27C, C110A)/H4, H3.2(C110A)/H4(Q27C).

Cysteine mutant H2A/H2B and H3.2/H4 tetramers were labeled with Oregon Green 488-maleimide (OG488) as previously described[80] with two additions of one molar equivalent of OG488 (Thermo Fisher) and purified again by cation exchange chromatography. The following fluorescently labeled, full-length histone complexes were prepared: H2A(A10C-OG488)/H2B = H2A*/H2B, H2A/H2B(A21C-OG488) = H2A/H2B*, H3.2(T32C-OG488, C110A)/H4 = H3*/H4, H3.2(C110A)/H4(Q27C-OG488) = H3/H4*, H2AΔAP/H2B(A21C-OG488) = H2AΔAP/H2B*.

The H2A/H2B*/Nap1 complex was reconstituted by mixing mNap1x1 and H2A/H2B* dimer at a 1:4 ratio in 20 mM Tris-Cl pH 8, 300 mM NaCl at a total protein concentration of 1 mg/ml. The reconstituted complex was purified away from excess H2A/H2B* dimer by size exclusion chromatography using a Superdex 200 increase 10/300 column (GE Healthcare) equilibrated in the same buffer. Pooled fractions were concentrated by centrifugal concentration (Vivaspin).

Bacterial expression plasmids encoding human histones with tail truncations were prepared using pST50Tr vectors as follows. H2A(1–97) (H2AΔC) was cloned using standard restriction enzyme and ligation methods. For histone N-terminal tail truncations (ΔN), the GSENLYFQGSGS (TEVGSGS, for non-labeled histones) or GSENLYFQGSCS (TEVGSCS, for labeled histones) was inserted in frame into the histone coding sequence at the following positions: H2A between residues 26 and 27 for both full-length (to make ΔN) and 1–97 (to make ΔNC) constructs, H2B between residues 35 and 36, H3.2 between residues 43 and 44, and H4 between residues 30 and 31. Gibson assembly was used to prepare H2A(1-26-TEVGSCS-27-97), H2A(1-26-TEVGSGS-27-129), H2B(1-35-TEVGSCS-36-125), H2B(1-35-TEVGSGS-36-125), H3.2(1-43-TEVGSCS-44-135), H3.2(1-43-TEVGSGS-44-135), H4(1-30-TEVGSCS-31-102), and H4(1-30-TEVGSGS-31-102). H2A(1-26-TEVGSGS-27-97) was cloned using standard restriction enzyme and ligation methods with a synthetic gblock template (IDT). These histones were expressed as described above for full-length histones and extracted from inclusion bodies. The following histone complexes were reconstituted and purified as described above: H2A(1-26-TEVGSCS-27-97)/H2B, H2B(1-35-TEVGSCS-36-125)/H2A, H2A(1-26-TEVGSGS-27-97)/H2B(A21C), H2A(1-26-TEVGSGS-27-129)/H2B(A21C), H2A(1-97)/H2B(A21C), H2A(A10C)/H2B(1-35-TEVGSGS-36-125), H3.2(1-43-TEVGSCS-44-135)/H4, H3.2(C110A)/H4(1-30-TEVGSCS-31-102), and H3.2(1-43-TEVGSGS-44-135)/H4(1-30-TEVGSGS-31-102). With the exception of H2A(1-97)/H2B(A21C), all of these histone complexes were cleaved with TEV protease and repurified by cation exchange chromatography. The resulting H3.2(GSGS-44-135)/H4(GSGS-31-102) = $H3^{\Delta N}/H4^{\Delta N}$ was used directly in mass photometry experiments. The remaining truncated histone complexes were fluorescently labeled

as described above to prepare H2A(GSCS-27-97-OG488)/H2B = H2A$^{\Delta NC*}$/H2B, H2B(GSCS-36-125-OG488)/H2A = H2A/H2B$^{\Delta N*}$, H2A(1-26-GSGS-27-97)/H2B(A21C-OG488) = H2A$^{\Delta NC}$/H2B*, H2A(GSGS-27-129)/H2B(A21C-OG488) = H2A$^{\Delta N}$/H2B*, H2A(1-97)/H2B(A21C-OG488) = H2A$^{\Delta C}$/H2B*, H2A(A10C-OG488)/H2B(1-35-GSGS-36-125) = H2A*/H2B$^{\Delta N}$, H3.2(GSCS-44-135-OG488)/H4 = H3$^{\Delta N*}$/H4, H3.2(C110A)/H4(GSCS-31-102-OG488) = H3/H4$^{\Delta N*}$.

All nucleosomes were assembled by gradient dialysis using the Widom 601 nucleosome positioning sequence[81] and purified by anion exchange chromatography using a Source Q resin (GE Healthcare) exactly as previously described[24,79]. Wild-type, H2AΔAP, and alanine mutant nucleosomes were assembled using 185 bp end biotinylated Widom 601 DNA (20 bp symmetric DNA linkers) for pulldown experiments[41]. H2A(E91C)/H2B was assembled with H3/H4 and 185 bp Widom 601 DNA (20 bp symmetric DNA linkers) for label transfer photocrosslinking experiments. Fluorescently labeled nucleosomes for ubiquitylation assays were assembled using H2A*/H2B or H2A/H2B* and H3/H4 or H2A/H2B and H3*/H4 or H3/H4* together with 147 bp Widom 601 DNA (1 bp symmetric DNA linkers). Wild type 185 bp nucleosomes were labeled with 5-(and-6)-carboxyrhodamine 6 G Succinimidyl Ester (Life Technologies) exactly as previously described[24] for APC/C-nucleosome pulldowns.

Histone tail peptides for ubiquitylation inhibition studies were generated recombinantly from chimeric fusion proteins. 10xHis-SUMO-H2A(1-26)-TEV-GSGS and 10xHis-SUMO-H3.2(1-43)-TEV-GSGS were synthesized as gblocks by IDT. Gibson assembly was used to prepare 10xHis-SUMO-H2A(1-26)-TEV-GSGS-eGFP and 10xHis-SUMO-H3.2(1-43)-TEV-GSGS-eGFP in the pST50Tr vector. Proteins were expressed in T7express lysY/iq cells (NEB) at 18 °C for 15 h. Cleared lysates were purified in batch using Talon resin, eluting with 200 mM imidazole. Fusion proteins were cleaved simultaneously with TEV protease and the Ulp1 SUMO protease for 15 h at 4 °C. The histone tail peptides were purified using a C18 column (Vydac) with a 0–73% B gradient over 45 min (buffer A: 0.1% trifluoroacetic acid (TFA), water; buffer B: 90% acetonitrile, 0.1% TFA, water). Pooled fractions were lyophilized and resuspended in water (H3.2) or 50% DMSO/water (H2A).

Nucleosome pulldowns

Nucleosome pulldowns using biotinylated nucleosome library and western blots were performed using HEK293T nuclear lysates exactly as previously described[41]. Input and eluted pulldown samples were run on 4–20% Criterion TGX gels (Bio-Rad) and transferred to nitrocellulose membranes (GE Healthcare) and western blots were performed with rabbit anti-APC2 (1:500, ABclonal, A8066), rabbit anti-APC5 (1:500, ABclonal, A7109), rabbit anti-CDC20 (1:500, ABclonal, A15656), or mouse anti-H3 (1:1,000, Cell Signaling Technologies, 3638S) primary antibodies and IRDye 800CW goat anti-rabbit IgG (1:10,000, LI-COR, 926-32211) or goat anti-mouse IgG (1:10,000, LI-COR, 926-32210) secondary antibodies. Western blots were imaged using an Odyssey imager (LI-COR).

Label transfer crosslinking

The H2A(E91C) nucleosome was reduced by addition of 1 mM TCEP to a 2 mg/ml solution of nucleosome in labeling buffer (20 mM HEPES pH 7.5, 20 mM NaCl) at room temperature for 30 min. The reducing agent was removed using a Zeba Spin desalting column equilibrated in labeling buffer. The nucleosome was labeled with Mts-Atf-Biotin (2-[N2-(4-Azido-2,3,5,6-tetrafluorobenzoyl)-N6-(6-biotinamidocaproyl)-L-lysinyl]ethyl Methanethiosulfonate; Santa Cruz Biotechnology) by addition of 10 molar equivalents of Mts-Atf-Biotin for 1 h at room temperature, protected from light. Unreacted Mts-Atf-Biotin was removed by repeating the Zeba Spin desalting step described above and nucleosomes were stored in labeling buffer with 20% glycerol at -80 °C until use.

For crosslinking experiments, 0.5 μM H2A-E91C-Atf-Biotin nucleosome was mixed with 1 μM APC/C in crosslinking buffer (10 mM HEPES pH 7.5, 75 mM NaCl) in a total volume of 20 μl. Irradiation was performed with samples on ice for 90 s using a model 66901 Thermo Oriel mercury lamp operating at 320 W with a 300–390 nm filter at a distance of 11 cm. Lamp output at 11 cm was measured at ~20 mW at 320 nm. Reduction of the label transfer reagent was performed by adding 50 mM DTT to gel loading dye and heating at 95 °C for 5 min. Four samples were prepared, one was irradiated and reduced, one was irradiated and not reduced, one was reduced and not irradiated, and one was neither irradiated nor reduced. Samples were run on a 4–20% Criterion TGX gel (Bio-Rad) and blotted with streptavidin 800 CW (LI-COR) at a 1:4000 dilution. A western blot was later performed with the same membrane using a mouse anti-APC3 antibody (1:10,000, Santa Cruz, SC-9972) and 680CW goat anti-mouse IgG secondary antibody (1:10,000, LI-COR) allowing simultaneous detection of the label transfer reagent and APC3. Blots were visualized using an Odyssey imager (LI-COR). Assay was replicated with equivalent results.

APC/C pulldowns

APC/C pulldowns were performed as previously described[24]. Briefly, 50 μl of 0.2 μM Twin Strep tagged APC/C (containing wild-type or 3RE APC3 and harboring glutamate substitutions described above) in binding buffer 200 (20 mM HEPES pH 7.5, 200 mM NaCl, 10% glycerol, 1 mM DTT, 0.1% NP-40) were bound to 150 μl MagStrep "type3" XT beads (IBA Lifesciences) equilibrated in the same buffer on a platform shaker for 60 min at 4 °C. Beads were washed twice with 500 μl binding buffer 200 and twice with binding buffer 75 (as above with 75 mM NaCl). 50 μl of 5 μM carboxyrhodamine labeled 185 bp nucleosome was added in binding buffer 75 to each immobilized APC/C or a beads only control and incubated as above. Following, five washes with binding buffer 75, bound proteins were eluted using 20 μl binding buffer 75 supplemented with 50 mM biotin shaking for 30 min at 4 °C. Input and eluted samples were separated using SDS-PAGE using an any kD Criterion gel (Bio-Rad) and visualized by fluorescence scanning and Coomassie staining.

Substrate ubiquitylation

Substrate ubiquitylation assays were performed at room temperature and quenched using SDS-containing sample buffer. Visualization of the ubiquitylated substrates involved separation by SDS-PAGE, and imaging using a Typhoon Fluorescence scanner. Ubiquitylation assays testing substrate polyubiquitylation of nucleosome or histone complexes were carried out by mixing 80 nM APC/C, 0.5 μM CDC20 or CDH1, 5 mM ATP/MgCl2, 1 μM UBA1, 2 μM UBE2C, 0.5 μM fluorescently labeled histone H2A/H2B dimer or H3/H4 tetramer, ± either 1 μM or 10 μM WDR5, ±30 μM Hsl1 D-box peptide or KEN-box peptide, or ± 10 μM UBE2SCTP. 125 μM Ub was added to start the reaction and quenched after 20 min. Substrate competition assays contained ± unlabeled H3/H4, Securin, or Cyclin B^{N} at increasing concentrations of 0.002, 0.02, 0.2, or 2 μM. Histone tail competition assays contained either ± H2A(1-26) N-terminal tail peptide at concentrations of 0.5, 5, or 15 μM, or ± H3(1-43) N-terminal tail peptide at concentrations of 0.5, 1.5, or 3 μM. Coactivator-independent assays testing histone dimer or tetramer ubiquitylation using APC/C, APC/C Plat, or APC/C Plat+APC8 were quenched after 2 h. Full gel scans and blots are available in the Source Data file. Positions of fluorescently labeled proteins are marked to designate molecular weights as molecular weight markers are not visible on fluorescence scans.

Mass spectrometry sample prep

Ubiquitylated histones prepared for mass spectrometry analysis were generated by incubating reaction components for 6 h at room temperature, using mixtures containing 0.4 μM APC/C, 1 μM CDC20, 1 μM

UBA1, 8 μM UBE2C, 5 μM unlabeled H2A/H2B dimer or H3/H4 tetramer, 0.5 μM fluorescently labeled H2A/H2B dimer or H3/H4 tetramer, and 125 μM of either Ub or methylated Ub. Reactions were quenched using a final concentration of 50 mM EDTA. Modified histones were isolated from the reaction components using ion-exchange chromatography resin. Samples were taken prior to and after the reaction, as well as during ion-exchange chromatography wash and elution steps for SDS-PAGE analysis and visualized using a Typhoon Fluorescence scanner. Assays were replicated a minimum of two times with equivalent results.

Mass spectrometry

Modification of lysines by propionylation was performed as previously described with some modifications[82]. Samples were dried to 0 via a SpeedVac concentrator and resuspended in 30 μL 100 mM ammonium bicarbonate (ABC). Propionylation reagent was prepared by adding 10 μL propionic anhydride (Millipore Sigma #240311) to 30 μL 2-propanol. 10 μL was immediately added to each sample. Samples were kept close to pH 8.0 by addition of 25% ammonia solution (Millipore Sigma #5.33003) and monitored using pH strips. Samples were then incubated at 37 °C for 15 min. Samples were dried down to 5–10 μL using a SpeedVac to remove unreacted propionic reagent and then brought back up to 30 μL with water. After adjustment back to pH 8.0, samples underwent another round of propionylation. Samples were then dried to 0 and resuspended in 100 μL 100 mM ABC. Samples were reduced with 5 mM DTT at 60 °C for 30 min and alkylated with 15 mM chloroacetamide at room temperature for 40 min. Samples were digested with 2.5 μg of trypsin for 17 h at 37 °C. The trypsin was then neutralized with 1 M HCl to a final concentration of 50 mM HCl and the samples were dried to 0 in a SpeedVac and then resuspended in 30 μL 100 mM ABC. Samples then underwent another round of propionylation as described above. After the final round, samples were dried to 0 and resuspended in 100 μL 0.5% Trifluoroacetic acid (TFA).

Samples were desalted using C-18 spin columns (Thermo Scientific #89870). The columns were wetted with 200 μL acetonitrile and equilibrated with 200 μL 0.5% TFA. Samples were then loaded onto the column and washed two times with 0.5% TFA. Samples were eluted off the column using 50 μL 70% acetonitrile, 0.1% TFA two times. The samples were dried to 0 and resuspended in 25 μL 98% water, 2% acetonitrile, 0.1% formic acid.

Peptides were separated via reverse-phase nano-HPLC using an RSLCnano Ultimate 3000 (Thermo Fisher Scientific). The mobile phase consisted of water + 0.1% formic acid as buffer A and acetonitrile + 0.1% formic acid as buffer B. Peptides were loaded onto a μPAC™ Trapping column (PharmaFluidics) and separated on a 50 cm μPAC™ column (PharmaFluidics) operated at 35 °C flowing at 300 nL/min using a segmented 60 min gradient as follows: 11 min from 2–12% buffer B and 49 min from 12 to 40% buffer B. Mass spectrometry analysis was performed on an Orbitrap Eclipse (Thermo Fisher Scientific) operated in data-dependent acquisition mode. MS1 scans were obtained at 120,000 resolution in the Orbitrap with a scan range from 375 to 2000 m/z, 50 ms max injection time, and automated gain control (AGC) target of 1e6. All precursors were filtered for monoisotopic peaks, charge states 2–7, and used a dynamic exclusion of 45 s with 10 ppm mass tolerance excluding isotopes. Precursors selected for MS2 were isolated in the quadrupole with an isolation window width of 0.7 m/z. MS2 ions were obtained in the Orbitrap at 15,000 resolution with 2 ms max injection time and 5e4 AGC and fragmented with higher-energy collision induced dissociation (HCD) collision energy of 35%. Each sample was analyzed in triplicate.

After data acquisition, raw files were processed for peptide identifications with MSFragger[83] (version 3.8) against the UniProtKB/Swiss-Prot homo sapiens sequence database (downloaded on August 2019) appended with contaminant sequences (20,681 sequences). The following parameters were used for an open search[84]: fully-tryptic digestion with ≤2 missed cleavages, and precursor mass tolerance of −150 to 500 Da. Fixed modifications were used for carbamidomethyl cysteine, propionylated lysine, and propionylated N-termini. Variable modifications consisted of oxidized methionine and acetylated protein N-termini. Identifications were filtered to a 1% FDR. Mass shifts corresponding to ubiquitylated peptides from histone proteins were manually inspected for quality and spectral counts were used for quantification. The mass spectrometry proteomics data have been deposited to the ProteomeXchange Consortium via the PRIDE partner repository with the dataset identifier PXD052680.

Cryo-EM sample preparation

H2A/H2B(K11C) and H3.2(K27C, C110A)/H4 were crosslinked to C-terminally Strep tagged UBE2C (C102A) using bis-maleimidoethane (BMOE, ThermoFisher) as previously described to prepare UBE2C-X-H2A/H2B and -X-H3/H4[48–50]. To reconstitute APC/C-CDC20-UBE2C-X-H2A/H2B, APC/C (1.1 μM), MYCx3-Hisx6-CDC20 (1.1 μM) and UBE2C-X-H2A/H2B (5.6 μM) were combined in 300 μl reconstitution buffer (10 mM HEPES pH 7.5, 100 mM NaCl, 1 mM DTT) and the complex was purified away from excess UBE2C-X-H2A/H2B by gel filtration chromatography using a Superose 6 increase 10/300 column (GE Healthcare) equilibrated in crosslinking buffer (10 mM HEPES pH 7.5, 50 mM NaCl, 1 mM DTT). APC/C-CDC20-H2A/H2B and APC/C-H2A/H2B complexes were prepared similarly. To prepare APC/C-CDC20-UBE2C-X-H3/H4, APC/C (1.2 μM), MYCx3-Hisx6-CDC20 (1.2 μM) and UBE2C-X-H3/H4 (1.5 μM) were combined in 300 μl reconstitution buffer and purified as described above. The APC/C complexes were crosslinked as previously described[85]. Briefly, glutaraldehyde was added to a final concentration of 0.1% for 5 min at room temperature, followed by quenching with addition of Tris-Cl pH 7.5 to a final concentration of 20 mM for an addition 10 min at room temperature. Finally, samples were buffer exchanged into crosslinking buffer without DTT using a Zeba spin desalting column and diluted to ~1 mg/ml for cryo-EM sample preparation. Crosslinked APC/C-CDC20-UBE2C-X-H2A/H2B (1.1 mg/ml) and APC/C-CDC20-UBE2C-X-H3/H4 (1 mg/ml supplemented with n-dodecyl-beta-maltoside at 0.125 critical micelle concentration) were applied to Quantifoil R1.2/1.3 300 mesh grids after treatment with a Tergeo EM plasma cleaner (60 s) and grids were frozen using a Vitrobot Mark IV with a 3 s blot time, 30 s wait time, and −10 blot force at 4 °C and 100% humidity.

The APC/C-CDC20-nucleosome complex was prepared by mixing nucleosome (2.4 μM), APC/C (0.48 μM) and MYCx3-Hisx6-CDC20 (0.48 μM) in 440 μl reconstitution buffer. The sample was crosslinked as above with 0.1% glutaraldehyde but the quenched sample was purified by gel filtration chromatography using a Superose 6 increase 10/300 column equilibrated in crosslinking buffer (GE Healthcare) and concentrated. Cryo-EM samples were prepared exactly as described for the APC/C-CDC20-UBE2C-X-H3/H4 complex.

Cryo-EM data collection and analysis

Imaging of grids was conducted on a Thermo Fisher Scientific 200 kV TEM Talos Arctica G3 equipped with a Gatan K3 direct electron detector. Sixty-frame movies were collected in counting mode using SerialEM with a multi-shot 5 × 5 regular pattern, at ×45,000 nominal magnification corresponding to a pixel size of 0.91 Å for APC/C-CDC20-UBE2C-X-H2A/H2B and APC/C-CDC20-nucleosome or 0.88 Å for APC/C-CDC20-UBE2C-X-H3/H4, a defocus range of −0.5 μm to −3.0 μm and a total dose of 42–50 $e^-/Å^2$. A small, yet quantifiable change in pixel size was noted in calibrations between collection of the datasets. A total of 10,028, 8505, and 2576 movies for APC/C-CDC20-UBE2C-X-H2A/H2B, APC/C-CDC20-UBE2C-X-H3/H4 and APC/C-CDC20-nucleosome were collected, respectively.

Movies were imported into RELION 3.1 based on the beam image shifts (optics groups) used for data collection. Motion correction and CTF estimation were conducted using the RELION implementation of MotionCor2 and CTFFIND-4.1, respectively, and only micrographs with an estimated resolution below 5 Å were used for further processing. All micrographs or a subset of 500 and 2500 micrographs from the APC/C-CDC20-nucleosme, APC/C-CDC20-UBE2C-X-H2A/H2B or APC/C-CDC20-UBE2C-X-H3/H4 datasets, respectively, were used in RELION Laplacian-of-Gaussian 2D classification to generate 2D classes for templated-based particle picking of the full dataset. 4 rounds of iterative Laplacian-of-Gaussian followed by 4 rounds of iterative templated-based 2D classification and one round of 3D classification resulted in initial reconstructions of the APC/C-CDC20-UBE2C-X-H2A/H2B and APC/C-CDC20-UBE2C-X-H3/H4. Only the iterative Laplacian-of-Gaussian 2D classification step was conducted for the APC/C-CDC20-nucleosome complex. The following processing steps were carried out in the RELION 4.0. The best 3D classes were selected for 3D refinement, followed by per-particle CTF refinement and another round of 3D refinement to yield high resolution model for 3D classification without alignment and regularization parameter set to 20. The highest resolution models were selected for 3D refinement followed by Bayesian particle polishing, per-particle CTF refinement and final 3D refinement using solvent-flattened FSCs. Local resolution, FSC curves, and angular distribution were calculated using RELION 4.0. Maps were low pass filtered at 10 Å using relion_image_handler.

To build the APC/C-CDC20-UBE2C-X-H3/H4 model, the APC/C-CDH1-UBE2C polyalanine model, 8TAU[51], was aligned to the final cryo-EM map using Chimera[86]. Chain R containing CDH1 was manually removed from this model. To obtain a starting model for CDC20, the APC/C-CDC20 model, 6Q6H, was also aligned to the map as above. Chain R containing CDC20 was converted to a polyalanine model using Chainsaw in CCP4[87]. An initial APC/C-CDC20 model was generated by combining these aligned polyalanine APC/C-UBE2C and CDC20 models. Real space refinement was performed in Phenix 1.20[88]. An H3ΔN/H4ΔN structure was generated from chains A and B of structure 3AFA[89] and was manually docked into the map using Chimera to give the final APC/C-CDC20-UBE2C-X-H3/H4 model. The APC/C-CDC20-UBE2C-X-H2A/H2B model was built similarly, starting with the refined APC/C-CDC20-UBE2C model above and using chains C and D of structure 3AFA.

Mass photometry

Mass photometry measurements were conducted on a Refeyn OneMP system (Refeyn Ltd) as described previously[90,91]. All sample components were mixed at twice the final concentration and incubated at room temperature for 5 min prior to final dilution and measurement. Measurements were carried out using buffer containing 20 mM HEPES pH 8, and 200 mM NaCl. Samples containing only APC/C were measured at a final concentration of 80 nM. Samples containing both APC/C and histones were measured at a final concentration of 160 nM APC/C and either 320 or 640 nM H2A/H2B dimer or H3/H4 tetramer. $N = 3$ replicates were recorded for each sample. Data was analyzed using DiscoverMP. Representative histograms fitted using kernel density estimates were generated using matplotlib (v3.8.3) from events exported out of DiscoverMP.

Reporting summary

Further information on research design is available in the Nature Portfolio Reporting Summary linked to this article.

Data availability

The mass spectrometry data used for ubiquitylation site identification has been deposited to the ProteomeXchange Consortium via the PRIDE partner repository with the dataset identifier PXD052680. Cryo-EM maps have been deposited in the Electron Microscopy Data Bank under accession codes EMD-48984 (APC/C-CDC20-UBE2C-X-H3/H4), and EMD-48928 (APC/C-CDC20-UBE2C-X-H2A/H2B). APC/C-CDC20-UBE2C models from H2B/H2B-bound and H3/H4-bound complexes have been deposited in the Protein Data Bank under the accession codes 9N9R and 9N9S, respectively. A previously published proteomics dataset was used in this study with dataset identifier PXD032791. Previously reported PDB entries 8TAU, 6Q6H, 8TAR, 5L9U, 5KHR, 5A31, and 3AFA, were used in this study. Models and materials used in this study are available upon request. Source data are provided with this paper.

References

1. McGinty, R. K. & Tan, S. Nucleosome structure and function. *Chem. Rev.* **115**, 2255–2273 (2015).
2. Luger, K., Mäder, A. W., Richmond, R. K., Sargent, D. F. & Richmond, T. J. Crystal structure of the nucleosome core particle at 2.8 Å resolution. *Nature* **389**, 251–260 (1997).
3. Millán-Zambrano, G., Burton, A., Bannister, A. J. & Schneider, R. Histone post-translational modifications - cause and consequence of genome function. *Nat. Rev. Genet.* **23**, 563–580 (2022).
4. Mattiroli, F. & Penengo, L. Histone ubiquitination: an integrative signaling platform in genome stability. *Trends Genet.* **37**, 566–581 (2021).
5. Vaughan, R. M., Kupai, A. & Rothbart, S. B. Chromatin regulation through ubiquitin and ubiquitin-like histone modifications. *Trends Biochem. Sci.* **46**, 258–269 (2021).
6. Komander, D. & Rape, M. The ubiquitin code. *Annu. Rev. Biochem.* **81**, 203–229 (2012).
7. Rape, M. Ubiquitylation at the crossroads of development and disease. *Nat. Rev. Mol. Cell Biol.* **19**, 59–70 (2018).
8. Yau, R. & Rape, M. The increasing complexity of the ubiquitin code. *Nat. Cell Biol.* **18**, 579–586 (2016).
9. Oh, E., Akopian, D. & Rape, M. Principles of ubiquitin-dependent signaling. *Annu. Rev. Cell Dev. Biol.* **34**, 137–162 (2018).
10. Singh, R. K. et al. Excess histone levels mediate cytotoxicity via multiple mechanisms. *Cell Cycle* **9**, 4236–4244 (2010).
11. Meeks-Wagner, D. & Hartwell, L. H. Normal stoichiometry of histone dimer sets is necessary for high fidelity of mitotic chromosome transmission. *Cell* **44**, 43–52 (1986).
12. Singh, R. K., Kabbaj, M.-H. M., Paik, J. & Gunjan, A. Histone levels are regulated by phosphorylation and ubiquitylation-dependent proteolysis. *Nat. Cell Biol.* **11**, 925–933 (2009).
13. Challa, K. et al. Damage-induced chromatome dynamics link Ubiquitin ligase and proteasome recruitment to histone loss and efficient DNA repair. *Mol. Cell* **81**, 811–829.e6 (2021).
14. Hauer, M. H. et al. Histone degradation in response to DNA damage enhances chromatin dynamics and recombination rates. *Nat. Struct. Mol. Biol.* **24**, 99–107 (2017).
15. Qian, M.-X. et al. Acetylation-mediated proteasomal degradation of core histones during DNA repair and spermatogenesis. *Cell* **153**, 1012–1024 (2013).
16. Shmueli, M. D., Sheban, D., Eisenberg-Lerner, A. & Merbl, Y. Histone degradation by the proteasome regulates chromatin and cellular plasticity. *FEBS J.* **289**, 3304–3316 (2022).
17. Xia, Y. et al. RNF8 mediates histone H3 ubiquitylation and promotes glycolysis and tumorigenesis. *J. Exp. Med.* **214**, 1843–1855 (2017).
18. Maze, I. et al. Critical role of histone turnover in neuronal transcription and plasticity. *Neuron* **87**, 77–94 (2015).
19. Baptista, T. et al. Regulation of histone H2A.Z expression is mediated by sirtuin 1 in prostate cancer. *Oncotarget* **4**, 1673–1685 (2013).
20. Chen, I.-Y. et al. Histone H2A.z is essential for cardiac myocyte hypertrophy but opposed by silent information regulator 2alpha. *J. Biol. Chem.* **281**, 19369–19377 (2006).

21. Fatima, A. et al. The ubiquitin-conjugating enzyme UBE2K determines neurogenic potential through histone H3 in human embryonic stem cells. *Commun. Biol.* **3**, 262–19 (2020).
22. Marzluff, W. F. & Koreski, K. P. Birth and death of histone mRNAs. *Trends Genet*. **33**, 745–759 (2017).
23. Oh, E. et al. Gene expression and cell identity controlled by anaphase-promoting complex. *Nature* **144**, 940 (2020).
24. Skrajna, A. et al. Comprehensive nucleosome interactome screen establishes fundamental principles of nucleosome binding. *Nucleic Acids Res.* **48**, 9415–9432 (2020).
25. McGinty, R. K. & Tan, S. Principles of nucleosome recognition by chromatin factors and enzymes. *Curr. Opin. Struct. Biol.* **71**, 16–26 (2021).
26. Bodrug, T., Welsh, K. A., Hinkle, M., Emanuele, M. J. & Brown, N. G. Intricate regulatory mechanisms of the anaphase-promoting complex/cyclosome and its role in chromatin regulation. *Front. Cell Dev. Biol.* **9**, 687515 (2021).
27. King, R. W., Deshaies, R. J., Peters, J. M. & Kirschner, M. W. How proteolysis drives the cell cycle. *Science* **274**, 1652–1659 (1996).
28. Yu, H., King, R. W., Peters, J. M. & Kirschner, M. W. Identification of a novel ubiquitin-conjugating enzyme involved in mitotic cyclin degradation. *Curr. Biol.* **6**, 455–466 (1996).
29. Aristarkhov, A. et al. E2-C, a cyclin-selective ubiquitin carrier protein required for the destruction of mitotic cyclins. *Proc. Natl. Acad. Sci. USA* **93**, 4294–4299 (1996).
30. Dimova, N. V. et al. APC/C-mediated multiple monoubiquitylation provides an alternative degradation signal for cyclin B1. *Nat. Cell Biol.* **14**, 168–176 (2012).
31. Wu, T. et al. UBE2S drives elongation of K11-linked ubiquitin chains by the anaphase-promoting complex. *Proc. Natl. Acad. Sci. USA* **107**, 1355–1360 (2010).
32. Garnett, M. J. et al. UBE2S elongates ubiquitin chains on APC/C substrates to promote mitotic exit. *Nat. Cell Biol.* **11**, 1363–1369 (2009).
33. Williamson, A. et al. Identification of a physiological E2 module for the human anaphase-promoting complex. *Proc. Natl. Acad. Sci. USA* **106**, 18213–18218 (2009).
34. McGinty, R. K., Henrici, R. C. & Tan, S. Crystal structure of the PRC1 ubiquitylation module bound to the nucleosome. *Nature* **514**, 591–596 (2014).
35. Witus, S. R. et al. BRCA1/BARD1 site-specific ubiquitylation of nucleosomal H2A is directed by BARD1. *Nat. Struct. Mol. Biol.* **28**, 268–277 (2021).
36. Hu, Q. et al. Mechanisms of RNF168 nucleosome recognition and ubiquitylation. *Mol. Cell* **84**, 839–853.e12 (2024).
37. Hu, Q. et al. Mechanisms of BRCA1-BARD1 nucleosome recognition and ubiquitylation. *Nature* **596**, 438–443 (2021).
38. Franks, J. L. et al. In silico APC/C substrate discovery reveals cell cycle-dependent degradation of UHRF1 and other chromatin regulators. *PLoS Biol.* **18**, e3000975 (2020).
39. Wang, H., Feng, K., Wang, Q. & Deng, H. Reciprocal interaction between SIRT6 and APC/C regulates genomic stability. *Sci. Rep.* **11**, 14253 (2021).
40. Ledvin, L. et al. The anaphase-promoting complex controls a ubiquitination-phosphoprotein axis in chromatin during neurodevelopment. *Dev. Cell* **58**, 2666–2683.e9 (2023).
41. Spangler, C. J. et al. Structural basis of paralog-specific KDM2A/B nucleosome recognition. *Nat. Chem. Biol.* **19**, 1–9 (2023).
42. Ueda, T., Catez, F., Gerlitz, G. & Bustin, M. Delineation of the protein module that anchors HMGN proteins to nucleosomes in the chromatin of living cells. *Mol. Cell. Biol.* **28**, 2872–2883 (2008).
43. Kato, H. et al. Architecture of the high mobility group nucleosomal protein 2-nucleosome complex as revealed by methyl-based NMR. *Proc. Natl. Acad. Sci. USA* **108**, 12283–12288 (2011).
44. Hammond, C. M., Strømme, C. B., Huang, H., Patel, D. J. & Groth, A. Histone chaperone networks shaping chromatin function. *Nat. Rev. Mol. Cell Biol.* **18**, 141–158 (2017).
45. Davey, N. E. & Morgan, D. O. Building a regulatory network with short linear sequence motifs: lessons from the degrons of the anaphase-promoting complex. *Mol. Cell* **64**, 12–23 (2016).
46. Burton, J. L. & Solomon, M. J. D box and KEN box motifs in budding yeast Hsl1p are required for APC-mediated degradation and direct binding to Cdc20p and Cdh1p. *Genes Dev.* **15**, 2381–2395 (2001).
47. Cirillo, L. et al. Spatial control of the APC/C ensures the rapid degradation of cyclin B1. *EMBO J.* **43**, 4324–4355 (2024).
48. Brown, N. G. et al. RING E3 mechanism for ubiquitin ligation to a disordered substrate visualized for human anaphase-promoting complex. *Proc. Natl. Acad. Sci. USA* **112**, 5272–5279 (2015).
49. Brown, N. G. et al. Dual RING E3 architectures regulate multiubiquitination and ubiquitin chain elongation by APC/C. *Cell* **165**, 1440–1453 (2016).
50. Yamaguchi, M. et al. Cryo-EM of mitotic checkpoint complex-bound APC/C reveals reciprocal and conformational regulation of ubiquitin ligation. *Mol. Cell* **63**, 593–607 (2016).
51. Bodrug, T. et al. Time-resolved cryo-EM (TR-EM) analysis of substrate polyubiquitination by the RING E3 anaphase-promoting complex/cyclosome (APC/C). *Nat. Struct. Mol. Biol.* **30**, 1663–1674 (2023).
52. Zhang, S., Tischer, T. & Barford, D. Cyclin A2 degradation during the spindle assembly checkpoint requires multiple binding modes to the APC/C. *Nat. Commun.* **10**, 3863–16 (2019).
53. Chang, L., Zhang, Z., Yang, J., McLaughlin, S. H. & Barford, D. Atomic structure of the APC/C and its mechanism of protein ubiquitination. *Nature* **522**, 450–454 (2015).
54. Martinez-Chacin, R. C. et al. Ubiquitin chain-elongating enzyme UBE2S activates the RING E3 ligase APC/C for substrate priming. *Nat. Struct. Mol. Biol.* **27**, 550–560 (2020).
55. West, M. H. & Bonner, W. M. Histone 2B can be modified by the attachment of ubiquitin. *Nucleic Acids Res.* **8**, 4671–4680 (1980).
56. Busch, H. & Goldknopf, I. L. Ubiquitin - protein conjugates. *Mol. Cell Biochem.* **40**, 173–187 (1981).
57. Lee, C. C., Li, B., Yu, H. & Matunis, M. J. Sumoylation promotes optimal APC/C activation and timely anaphase. *ELife* **7**, e29539 (2018).
58. Eifler, K. et al. SUMO targets the APC/C to regulate transition from metaphase to anaphase. *Nat. Commun.* **9**, 1119–15 (2018).
59. Liu, W. et al. Lactate regulates cell cycle by remodelling the anaphase promoting complex. *Nature* **616**, 790–797 (2023).
60. Qiao, R. et al. Mechanism of APC/CCDC20 activation by mitotic phosphorylation. *Proc. Natl. Acad. Sci. USA* **113**, E2570–E2578 (2016).
61. Zhang, S. et al. Molecular mechanism of APC/C activation by mitotic phosphorylation. *Nature* **533**, 260–264 (2016).
62. Fujimitsu, K., Grimaldi, M. & Yamano, H. Cyclin-dependent kinase 1-dependent activation of APC/C ubiquitin ligase. *Science* **352**, 1121–1124 (2016).
63. Ghoneim, M., Fuchs, H. A. & Musselman, C. A. Histone tail conformations: a fuzzy affair with DNA. *Trends Biochem. Sci.* **46**, 564–578 (2021).
64. Morrison, E. A., Bowerman, S., Sylvers, K. L., Wereszczynski, J. & Musselman, C. A. The conformation of the histone H3 tail inhibits association of the BPTF PHD finger with the nucleosome. *eLife* **7**, e78587 (2018).
65. Clapier, C. R., Iwasa, J., Cairns, B. R. & Peterson, C. L. Mechanisms of action and regulation of ATP-dependent chromatin-remodelling complexes. *Nat. Rev. Mol. Cell Biol.* **18**, 407–422 (2017).
66. Kireeva, M. L. et al. Nucleosome remodeling induced by RNA polymerase II: loss of the H2A/H2B dimer during transcription. *Mol. Cell* **9**, 541–552 (2002).

67. Kulaeva, O. I. et al. Mechanism of chromatin remodeling and recovery during passage of RNA polymerase II. *Nat. Struct. Mol. Biol.* **16**, 1272–1278 (2009).
68. Filipovski, M., Soffers, J. H. M., Vos, S. M. & Farnung, L. Structural basis of nucleosome retention during transcription elongation. *Science* **376**, 1313–1316 (2022).
69. Ehara, H., Kujirai, T., Shirouzu, M., Kurumizaka, H. & Sekine, S.-I. Structural basis of nucleosome disassembly and reassembly by RNAPII elongation complex with FACT. *Science* **377**, eabp9466 (2022).
70. Ramachandran, S., Ahmad, K. & Henikoff, S. Transcription and remodeling produce asymmetrically unwrapped nucleosomal intermediates. *Mol. Cell* **68**, 1038–1053.e4 (2017).
71. Rhee, H. S., Bataille, A. R., Zhang, L. & Pugh, B. F. Subnucleosomal structures and nucleosome asymmetry across a genome. *Cell* **159**, 1377–1388 (2014).
72. Karl, L. A., Peritore, M., Galanti, L. & Pfander, B. DNA double strand break repair and its control by nucleosome remodeling. *Front. Genet.* **12**, 821543 (2021).
73. Mendiratta, S., Gatto, A. & Almouzni, G. Histone supply: multitiered regulation ensures chromatin dynamics throughout the cell cycle. *J. Cell Biol.* **218**, 39–54 (2019).
74. Alfieri, C., Tischer, T. & Barford, D. A unique binding mode of Nek2A to the APC/C allows its ubiquitination during prometaphase. *EMBO Rep.* **21**, e49831 (2020).
75. Alfieri, C. et al. Molecular basis of APC/C regulation by the spindle assembly checkpoint. *Nat. Struct. Mol. Biol.* **536**, 431–436 (2016).
76. Sedgwick, G. G. et al. Mechanisms controlling the temporal degradation of Nek2A and Kif18A by the APC/C-Cdc20 complex. *EMBO J.* **32**, 303–314 (2013).
77. Hames, R. S., Wattam, S. L., Yamano, H., Bacchieri, R. & Fry, A. M. APC/C-mediated destruction of the centrosomal kinase Nek2A occurs in early mitosis and depends upon a cyclin A-type D-box. *EMBO J.* **20**, 7117–7127 (2001).
78. Brown, N. G. et al. Mechanism of polyubiquitination by human anaphase-promoting complex: RING repurposing for ubiquitin chain assembly. *Mol. Cell* **56**, 246–260 (2014).
79. Luger, K., Rechsteiner, T. J. & Richmond, T. J. Preparation of nucleosome core particle from recombinant histones. *Methods Enzymol.* **304**, 3–19 (1999).
80. Budziszewski, G. R. et al. Multivalent DNA and nucleosome acidic patch interactions specify VRK1 mitotic localization and activity. *Nucleic Acids Res.* **50**, 4355–4371 (2022).
81. Lowary, P. T. & Widom, J. New DNA sequence rules for high affinity binding to histone octamer and sequence-directed nucleosome positioning. *J. Mol. Biol.* **276**, 19–42 (1998).
82. Lin, S. & Garcia, B. A. Examining histone posttranslational modification patterns by high-resolution mass spectrometry. *Methods Enzymol.* **512**, 3–28 (2012).
83. Kong, A. T., Leprevost, F. V., Avtonomov, D. M., Mellacheruvu, D. & Nesvizhskii, A. I. MSFragger: ultrafast and comprehensive peptide identification in mass spectrometry-based proteomics. *Nat. Methods* **14**, 513–520 (2017).
84. Yu, F. et al. Identification of modified peptides using localization-aware open search. *Nat. Commun.* **11**, 4065–4069 (2020).
85. Spangler, C. J. & McGinty, R. K. Determination of histone methyltransferase structures in complex with the nucleosome by cryogenic electron microscopy. *Methods Mol. Biol.* **2529**, 149–168 (2022).
86. Pettersen, E. F. et al. UCSF Chimera–a visualization system for exploratory research and analysis. *J. Comput Chem.* **25**, 1605–1612 (2004).
87. Agirre, J. et al. The CCP4 suite: integrative software for macromolecular crystallography. *Acta Crystallogr. D. Struct. Biol.* **79**, 449–461 (2023).
88. Afonine, P. V. et al. Real-space refinement in PHENIX for cryo-EM and crystallography. *Acta Crystallogr. D. Struct. Biol.* **74**, 531–544 (2018).
89. Tachiwana, H. et al. Structural basis of instability of the nucleosome containing a testis-specific histone variant, human H3T. *Proc. Natl. Acad. Sci. USA* **107**, 10454–10459 (2010).
90. Burnap, S. A. & Struwe, W. B. Mass photometry reveals SARS-CoV-2 spike stabilisation to impede ACE2 binding through altered conformational dynamics. *Chem. Commun.* **58**, 12939–12942 (2022).
91. Sonn-Segev, A. et al. Quantifying the heterogeneity of macromolecular machines by mass photometry. *Nat. Commun.* **11**, 1772–10 (2020).

Acknowledgements

Single particle cryo-EM data were collected with assistance from Jared Peck and Dr. Joshua Strauss at the University of North Carolina at Chapel Hill School of Medicine Cryo-Electron Microscopy Facility, which is partially supported by NIH P30CA016086 and is part of the Molecular Microscopy Consortium of the University of North Carolina at Chapel Hill, Duke University, and the NIEHS. Plasmids containing 601 nucleosome positioning DNA fragments were gifts from Song Tan. We thank members of the McGinty and Brown laboratories for critical comments on the manuscript. Molecular graphics and analyses were performed with UCSF Chimera, developed by the Resource for Biocomputing, Visualization, and Informatics at the University of California, San Francisco, with support from NIH P41-GM103311. This work was supported by NIH grants R35GM133498 to R.K.M., R35GM128855 to N.G.B., T32GM148376-01A1 to C.B.F., NSF DGE-1650116 to T.B. and American Cancer Society grant 132609-PF-18-153-01-DMC to A.S., and American Heart Association grant 23PRE1025746 to K.A.W.

Author contributions

R.K.M., N.G.B., D.G., D.S.L. supervised the studies. A.S., T.B., R.C.M.C., R.K.M. and N.G.B. conceived the study and designed the experiments. A.S. prepared samples, grids, collected and processed the cryo-EM data, and performed assays. T.B. prepared samples, processed the cryo-EM data, and performed assays. R.C.M.C., and C.B.F., and K.A.W. prepared samples and performed assays. Z.P. performed mass spectrometry experiments. A.N. and D.G. processed proteomics data., H.C.S., E.C.A., J.M.S., M.A.N., M.T.H., and I.F. prepared samples. Y.Z. and J.G.W. performed assays. A.S., T.B., R.K.M. and N.G.B. wrote the manuscript with contributions from all coauthors.

Competing interests

The Brown laboratory receives research funding from Amgen. The remaining authors declare no competing interests.

Additional information

Supplementary information The online version contains supplementary material available at https://doi.org/10.1038/s41467-025-57384-7.

Correspondence and requests for materials should be addressed to Nicholas G. Brown or Robert K. McGinty.

Peer review information *Nature Communications* thanks the anonymous reviewer(s) for their contribution to the peer review of this work. A peer review file is available.